KONA Powder and Particle Journal No. 40 (2023) 29–49/https://doi.org/10.14356/kona.2023002 Review Paper

Interfacial Engineering of Particulate & Surfactant Systems for Enhanced Performance in Industrial Applications †

Jiaqi Dong and Brij M. Moudgil *

Center for Particulate and Surfactant Systems (CPaSS), Department of Materials Science and Engineering, University of Florida, USA

Abstract

Particulate and surfactant systems are an integral part either in processing or product lines in essentially every major industry, including Energy and Minerals, Pharmaceutical, Agriculture & Food, Microelectronics, Healthcare, Cosmetics, Consumer Products, and Analytical Instrumentation & Services. In most applications, product and process specifications depend on the synergistic or competitive interactions between the particles and reagent schemes. The primary goal of our research efforts has been to generate the structure-property-performance correlations-based knowledge and technology platforms for industry to develop more sustainable products and processes. Engineering the physicochemical/mechanical properties of surfaces, particles, and self-assembling surfactant systems enables their enhanced performance in industrial applications. Specifically, understanding and control of the nano and atomic-scale forces between particles and synthesis of functionalized particles form the foundation for targeted contributions in biomedical, advanced materials and minerals, sensor, and coating technologies. A synoptic overview of selected projects is presented in this review. Additional details can be found in the topic-specific references listed at the end of this manuscript.

Keywords: interfacial engineering, functionalized particles, antibacterial coatings, antiscalant additives, corrosion inhibitors, precision particles

1. Introduction

Over the last few decades, the theme of research at the Particle Engineering Research Center (PERC) and subsequently at the Center for Particulate and Surfactant Systems (CPaSS—NSF Industry/University Cooperative Research Center) has been focused on developing the structure-property-performance correlations in the particle and surfactant systems. In most projects, control of forces between particles in suspensions and functionalization of particles form the foundation of targeted advances in separations, dispersion & flocculation, and coating technologies.

2. Synopsis of selected research topics

2.1 Competitive adsorption

Controlled adsorption of molecules on selected particles or moieties is necessary for achieving the desired separation of minerals, and also for the release of active ingredients in drug formulations. Center researchers have devoted considerable efforts to understand the selectivity principles and develop guidelines for achieving selective coatings of surfactant/polymers on targeted surfaces. For example, Engelhard Corporation has commercialized the "site blocking agent" concept developed in our research (Behl et al., 1993; 1996). Researchers in the pharmaceutical industry and microelectronic manufacturing, especially chemical mechanical polishing (CMP) slurry developers have also recognized the relevance and significance of our work on competitive (selective) adsorption of polymer and surfactant molecules.

The synthesis of functional particles has been a major focus of the Center research endeavors. An inorganic crystalline Cryptomelane type hydrous manganese dioxide was synthesized and successfully evaluated in ion exchange columns for selective removal of potassium ions from sodium ions. The synthesis protocol of this material was designed based on the "ion memory effect" displayed by specific minerals. Selective uptake by such functional materials is achieved by controlling the spatial arrangement of the structural ions. The objective of this work was to design an environmentally-benign water recycling technique in paper manufacturing (Prakash and Moudgil, 1995).

A novel flotation process based on in-situ generation of gas bubbles on the ink particles as they detach from the fibers was developed to deink wastepaper by PERC researchers (El-Shall et al., 2005).

† Received 3 August 2021; Accepted 24 November 2021
J-STAGE Advance published online 29 January 2022
* Corresponding author: Brij M. Moudgil;
Add: 1180 Center Drive, Gainesville, FL 32603, USA
E-mail: bmoudgil@perc.ufl.edu
TEL: +1-352-846-1194 FAX: +1-352-846-1196

2.2 Dispersion and flocculation—science and technology

Efforts to optimize CMP slurries revealed, to our knowledge, for the first time that shear and normal forces between particles and surfaces must be controlled independently of each other to achieve maximum removal rate with minimal defects (Basim et al., 2003). Additionally, selective adsorption of surfactants on various wafer components formed the basis of next-generation selective polishing slurries later commercialized by a university spin-off company. These findings also led to the development of reagent schemes for controlling the structure of particulate agglomerates (flocs) for the dewatering of suspensions. Additionally, the development of the theoretical basis and experimental measurements of mechanical properties of self-assembled surfactant structures, such as micelles at interfaces, revealed that specific materials could catalyze the structure formation process on surfaces at a lower concentration than in the bulk (Rabinovieh et al., 2005 and Singh et al., 2001). Based on this work, new reagent schemes were proposed for wafer polishing slurries and for crystal habit modification additives.

The synthesis of nanoscale rough surfaces coupled with modeling the effect of nanoscale roughness and humidity on interparticle forces have provided new insights into aggregation and dry dispersion phenomena important to devising the dedusting schemes (Rabinovich et al., 2002).

2.3 Cross-contamination in powder mixtures

Changes in the particulate behavior in a mixture under storage and handling have been an enigma to scientists in the past. It has been well known that particulate systems can exhibit different bulk behavior even when the physical and surface chemical properties such as shape and size, size distribution, zeta potential, and viscosity of the systems are similar. In this regard, research on cross-contamination of powders has shown that even slight contact between two solid surfaces may be sufficient for atomic/nanoscale material transfer from one surface to the other, thereby reducing the selectivity of reagent coatings on the two surfaces. When apatite and dolomite particles were gently mixed, the transfer of material was too small to be detected by conventional surface analytical tools such as EDA, ESCA, SEM, TEM, but was sufficient to result in measurable changes in their zeta potential. It was further determined that the cross-contamination in particulate mixtures could be controlled with chemical additives (Mehta N, 1993).

2.4 Polyhydroxy fullerenes (PHF)—their novel properties and applications

A new phenomenon, namely the optical ignition of poly hydroxyl fullerenes (PHF), was discovered in our laboratory (Krishna et al., 2010; 2016a). This discovery led to the synthesis of carbon nanostructures without the use of any metal catalysts (Krishna et al., 2010). It resulted in practical uses of PHF in designing new antimicrobial coatings, selective ablation of cancerous cells, new herbicides, and plant growth promoters. (Gao et al., 2011; 2016; Krishna et al., 2015; 2016b; Sharma et al., 2013a).

2.5 Effect of kaolin clays on casting rate

In a recently completed project on the engineering of clays, the characterization of clay samples from different locations revealed that morphology, crystallinity, and shape of the clay particles play a major role in the dewatering behavior and casting rate of ceramic products. (Badr et al., 2021).

2.6 Science and technology of odor control

In an odor control study, porous silica particles impregnated with nano copper deposits were reported to be much more efficient odor control materials. However, challenges were encountered by an industry partner when attempts were made to scale up the process. A systematic characterization of the product formulation steps revealed that not only the chemical composition of the copper catalyst but also the morphology of the nano deposits in the pores played a critical role in achieving the optimal product performance (Singh et al., 2010).

3. Review highlights of selected research themes

3.1 Particle assisted removal of microbes from surfaces

In general, antibiotic-based strategies have limited efficacy owing to bacterial persistence and resistance to antibiotics. As a result, there has been an alarming growth of multi-drug-resistant pathogens. It is well known that non-alcohol-based cleansing formulations although may reduce 99.9 %+ bacteria and yet leave enough bacteria to cause infection. The need for alternative approaches has never been greater. The current project aimed at the removal of microbes rather than killing them.

Proper handwashing using soap, as per CDC guidelines, is quite effective. Soap molecules can outright kill the microbes or decrease the force of adhesion between the microbe and the skin. However, quite often in practice, due to lack of time, water or soap, improper handwashing can leave enough microbes on the skin to cause infections. Choices of more effective antimicrobial soaps are restricted due to health and safety regulations. Alcohol-based sanitizers are known to kill all microbes, but their repeated use without the application of skin emollients can lead to an increased risk of infection due to skin damage. For these reasons, engineered particles were developed to achieve higher efficacy of soap-based handwashing practices.

Considering that the microbes are negatively charged, the proposed hypothesis was investigated using positively

charged (cationic) silica particles. Silica particles (isoelectric point around pH of 2.8) are negatively charged under natural pH conditions (about pH 5.6) and can exhibit a positive charge when coated with polyethyleneimine (PEI). *E. coli* and VITRO-SKIN® served as the bacteria and skin surface, respectively. A brief description of the experimental procedures is given below. Additional details are provided in Nandakumar (2018).

Materials and reagents employed in this study and their respective sources (in parenthesis) are as follows: Silica of different particle sizes and Polyethyleneimine—M_n10,000 (Sigma-Aldrich, USA); Ampicillin sodium salt and Neutralizer D/E broth (Thermo Fisher Scientific); Artificial skin substrate -VITRO-SKIN® (IMS Inc. USA); *Escherichia coli*—ATCC 25922GFP (ATCC).

In order to remove any organic contaminants from the obtained silica surface, 1 g of the particles were treated with 1 M HCl for 60 min and thoroughly washed before conditioning with 40 mL of 2 wt % polyethylene imine—PEI, at pH 10.5 for 17 hours in a rotisserie. After recovering the PEI coated silica particles via centrifugation and washing them to remove excess PEI, they were lyophilized using a LABCONCO® freeze drier for storage purposes. Modified or unmodified silica particle suspensions were prepared in 0.5 % Tween 80 solution unless otherwise noted.

Brookhaven ZetaPlus®, and Coulter® LS13320 were employed for zeta potential and particle size measurements, respectively. For determining the amount of polymer coating, elemental analysis on a Carlo Erba NA1500 CNHS elemental analyzer was employed.

As per manufacturers protocol, 1.5 cm × 1.5 cm patch of VITRO-SKIN® was hydrated overnight using glycerol: water (15:85) binary mixture in a humidity chamber. Anton Paar® Physica Electro Kinetic Analyzer was used to measure the zeta potential. Surface energy was determined via contact angle measurements with water, glycerol, ethylene glycol, and diiodomethane, using the Owens-Wendt model (Owens and Wendt, 1969).

The surface energy of the *E. coli* strain (ATCC 25922GFP) was determined using a light scattering technique described elsewhere (Zhang X. et al., 2015). MATS (Microbial Adhesion to Solvents) assays were used to study the bacterial cell surface properties, including hydrophobic components and electron donor groups according to the protocol established (Bellon-Fontaine et al., 1996; Hamadi and Latrache, 2008). Bacterial adhesion to solvent was estimated by Eq. (1) (Bellon-Fontaine et al., 1996), where A_0 is the optical density at 600 nm of the aqueous suspension before mixing, A is the optical density of the aqueous suspension after mixing with the solvent pair.

$$\%\ adherence = \left(1 - \frac{A}{A_0}\right) * 100 \tag{1}$$

Interactions of modified and unmodified silica particles with bacteria were assessed by enumerating remnant bacterial population on the substrate following treatment with particles. Removal efficacy was calculated using Eq. (2).

$$\begin{aligned} &\log_{10} bacterial\ removal \\ &= \log_{10} Inoculum\ on\ skin \\ &\quad - \log_{10} bacteria\ remaining\ on\ skin \end{aligned} \tag{2}$$

The plate count method was used to estimate the cell density in the suspension, and the results were reported in terms of the total number of bacteria recovered as CFU. A wide-field fluorescence microscope (Cytation 5) was employed to assess cell membrane damage and cell viability.

In order to determine the extent of bacterial killing by the particles, tests were conducted by contacting the modified silica particles with *E. coli.* The cell viability illustrated in **Fig. 1** established that the modified particles by themselves do not kill the bacteria and hence would be suitable for removal studies.

Test results plotted in **Fig. 2** demonstrated that modified silica particles interact strongly with *E. coli* cells and can reduce bacterial concentrations by four log orders in 30 seconds in contrast to a maximum of 1.5 log reduction with unmodified control particles.

3.2 Particle design parameters for the removal of *E. coli* from artificial skin

A major hypothesis of this study was that microbial removal is possible only if the particle-bacterial interactions are strong enough to overcome the bacterial–substrate adhesion forces. Furthermore, particle size and density should be such that they impart enough shear force to remove the microbe-particle construct from the skin under handwashing conditions (e.g., fluid velocity, the volume of water, or time—20 seconds). Additionally, there need to be enough particles (particle loading, wt %) in the

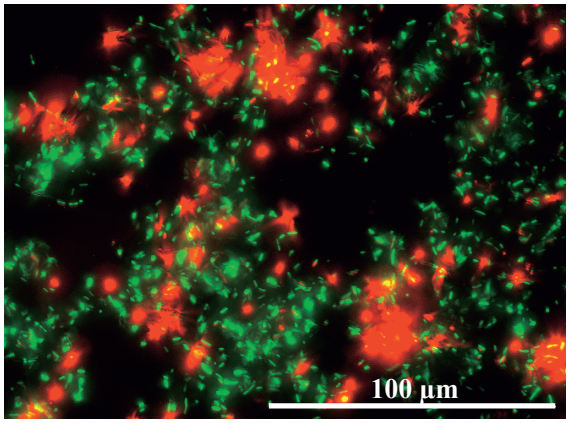

Fig. 1 Viability of microbes when attached to modified particles using fluorescence microscopy. Green—viable microbes attached to particles. Red—inactive microbes (Red intensity enhanced). Reprinted with permission from Ref. (Nandakumar et al., 2019). Copyright: (2019) Elsevier.

system to efficiently cleanse the skin. Accordingly, the role of adhesion forces (zeta potential), particle size, fluid velocity, and particle loading were systematically evaluated (Nandakumar et al., 2019).

It is observed from **Fig. 2** that an additional 2.5 log bacterial reduction on the skin surface is possible with the modified particles. It was further determined that the removal of bacteria dispersed on the skin (e.g., *E. coli*) was easier than the aggregated ones, e.g., *S. aureus*, see **Fig. 3** (Nandakumar, 2018).

Overall, this approach exhibited the potential of using modified particles to remove bacteria from surfaces as an alternative to kill-based methodologies.

3.3 Microbial disease control in the citrus plants: controlled release of insect repellants

In the past, engineered particle coatings have been successfully employed to control plant diseases in pear, apple, and cotton plants. Particle coatings of foliage primarily compromise the ability of insects to visualize, settle, feed, move and oviposit. They can also mask the color of the leaves and stems, making it difficult for insects to recognize them from a distance (Grafton-Cardwell et al., 2013; Glenn, 2012; Puterka et al., 2005; Wenninger et al., 2009). Sometimes the films themselves can be toxic to insects.

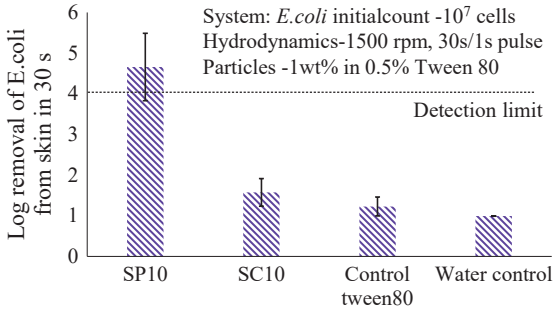

Fig. 2 Removal of *E. coli* using modified and unmodified silica particles. Reprinted with permission from Ref. (Nandakumar et al., 2019). Copyright: (2019) Elsevier.

Center researchers were approached to study the potential of particle coatings for managing the "Citrus Greening" diseases, which was detected by the Florida citrus growers back in 2005. "Citrus greening" (also known as the Huanglongbing or HLB) is a bacterial disease transmitted by an insect, the Asian citrus Psyllid (ACP). ACP attacks the younger flush making them more prone to infection, thus increasing the vulnerability of citrus trees during flush. The disease reduces the quality and quantity of the fruit yield, thereby threatening the economic viability of the Florida citrus industry. Some of the methods used and/or suggested to control citrus greening are as follows:

- Spraying of insecticides to control the insect attack. However, repetitive applications are required.
- Quarantine of infected trees, although it controls the spreading of the disease, the cost is a major drawback.
- Applying particulate (kaolin clay) coatings is effective in suppressing the disease, but rain fastness and exposure due to leaf growth remain major challenges.

Kaolin-based coatings have been reported to control the spread of the disease to varying degrees of success. However, the development of gaps upon the growth of leaves and washing off the coatings due to rains reduce their effectiveness for protection from the insects. Interestingly, contrary to conventional thinking, particle coatings are not only non-phytotoxic, but they improve water use efficiency. Hydrophobized Kaolin films have been shown to reduce heat stress by reflecting sunlight from the white film surface, and the porous nature of the films allows efficient gaseous exchange, thereby maintaining healthy photosynthesis in the plants (Glenn and Puterka, 2004; Puterka et al., 2005).

A systematic study was conducted to overcome a major limitation of the emerging gaps in the coatings due to leaf growth. Two approaches were proposed to overcome this challenge (i) developing a coating that slowly released an insect repellant such as garlic oil and (ii) coating the foliage with colored clays that masked the olfactory cues,

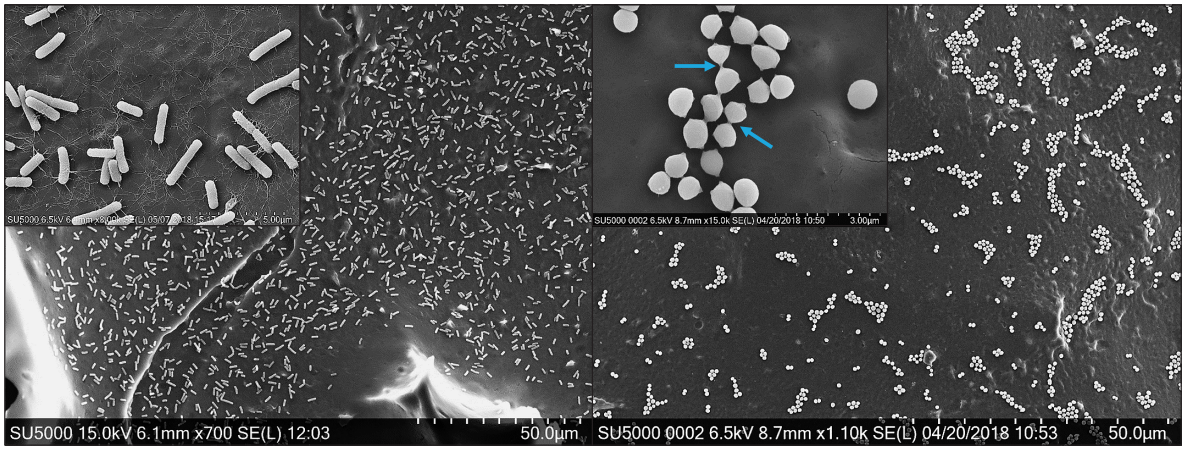

Fig. 3 *E. coli*—dispersed on skin **(left)**; *S. aureus*—agglomerated on skin **(right)**.

thus keeping the insects away from the citrus trees. These coatings were to also incorporate additives that enhance the rain fastness of the particles to the leaves.

3.4 Encapsulation of garlic oil (insect repellent) in unmodified and modified clays

The uptake of garlic oil (GO) was investigated using modified montmorillonite (MMT), surfactant treated montmorillonite (NMMT), and Claytone® 40 (hydrophobized montmorillonite). Pristine kaolin clays were employed as the negative control.

Fig. 4 shows that the highest uptake of GO was achieved in modified MMT clays such as Claytone 40 and NMMT (0.4 g GO/g clay), followed by unmodified MMT (0.2 g GO/g clay). The uptake of GO in pristine kaolin clays is almost negligible (0.04 g GO/g clay), possibly due to the lack of intergallery spacing and the hydrophilic nature of the kaolin clays (Narayanan et al., 2012; Sharma et al., 2013b).

Among the montmorillonite clays, the trend is consistent with the intergallery spacings (d_{001}) measured with the help of an X-ray diffractometer—Claytone 40 > NMMT > MMT. The increase in the intergallery spacing of Claytone 40 (29 Å) in the presence of GO (34 Å) suggests possible encapsulation of GO in between the layers. Similar results have also been reported in the literature for the sorption of aromatic compounds in Claytone 40. These set of experiments reinforced our hypothesis that the intergallery spacings and the hydrophobic nature of the clays are important for the integration of GO to the clays.

3.5 Release profile of encapsulated garlic oil

Preliminary data of release profile of GO from the clays is plotted in **Fig. 5**. The cumulative release of GO after four days from Claytone 40 is 13 % of the total encapsulated garlic oil (0.4 g/g of clay) as compared to 34 % of 0.2 g of GO uptaken in 1 g of unmodified MMT, and 84 % GO alone. It is hypothesized that uptake of GO in the clays is primarily due to electrostatic attraction between the modified clays and the garlic oil, along with uptake of GO within the hydrophobic pores. This study indicated the potential of controlled release of insect repellants as a methodology for crop protection purposes (Sharma et al., 2013b).

3.6 Colored clays as an optical and physical deterrent for insect attack of citrus plants

This project aimed to investigate if colored clays with reflectance in the visible range can prevent feeding on the citrus leaves by the Asian Citrus Psyllid (ACP), especially feeding on the fresh flush (fresh leaves). Colored kaolin clays were formulated using select dyes, including FDA-certified colorants, and approved for agricultural use by the EPA (list §180.920).

Basic dyes were used to prepare the colored kaolin clays (Moudgil et al., 2017; Sharma et al., 2015). Several clays from different suppliers were evaluated, and only a white clay sample was selected for further processing. Clay particles surfaces were modified using cationic surfactants and/or polymers, followed by mixing them with the dyes. This step was essential to prevent the leaching of the dyes from the clay particle suspensions. Zeta potential of the unmodified clays was determined to be about –31 mV and changed to +5 mV to +22 mV when treated with the acidic dyes, and –13 mV to –23 mV upon treatment with the basic dyes. Zeta potential was measured using a Zeta Plus Analyzer from Brookhaven instruments.

Ten different colored clays were developed using dyes—FD&C Blue 1, FD&C Red 40, Basic Blue 54, Crystal Violet, and FD&C Yellow 6, D&C Violet 2, as shown in **Fig. 6**. The optical properties of the colored clays were characterized using an integrating sphere (Lambda 800 UV-vis Spectrometer) for total reflectance measurements. These measurements were carried out by depositing a clay film on a glass slide.

It was determined that the majority of the colored clay coatings increased the reflectance in the 400–500 nm range relative to the uncoated leaves. The colorant strength of the

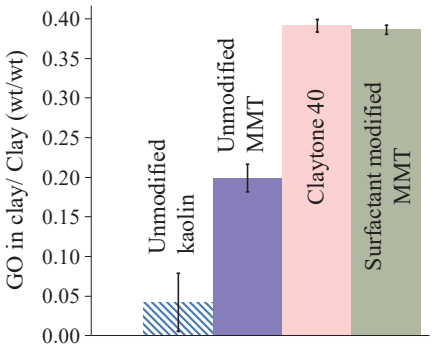

Fig. 4 Uptake of GO in unmodified MMT, modified MMT, and unmodified kaolin clays (clay = 1 g; the initial amount of GO = 0.4 g) (error bars with one std dev). Reprinted with permission from Ref. (Sharma et al., 2013b). Copyright: (2013) The Authors, patented in U.S.

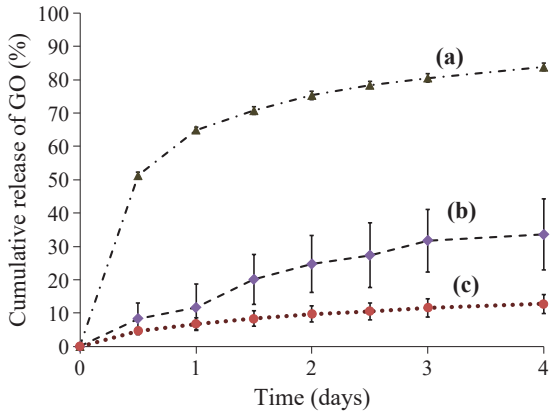

Fig. 5 The release profile of **(a)** GO alone, **(b)** GO from unmodified MMT, and **(c)** GO from Claytone 40. (Temp 22 °C; error bars with one std. deviation). Reprinted with permission from Ref. (Sharma et al., 2013b). Copyright: (2013) The Authors, patented in U.S.

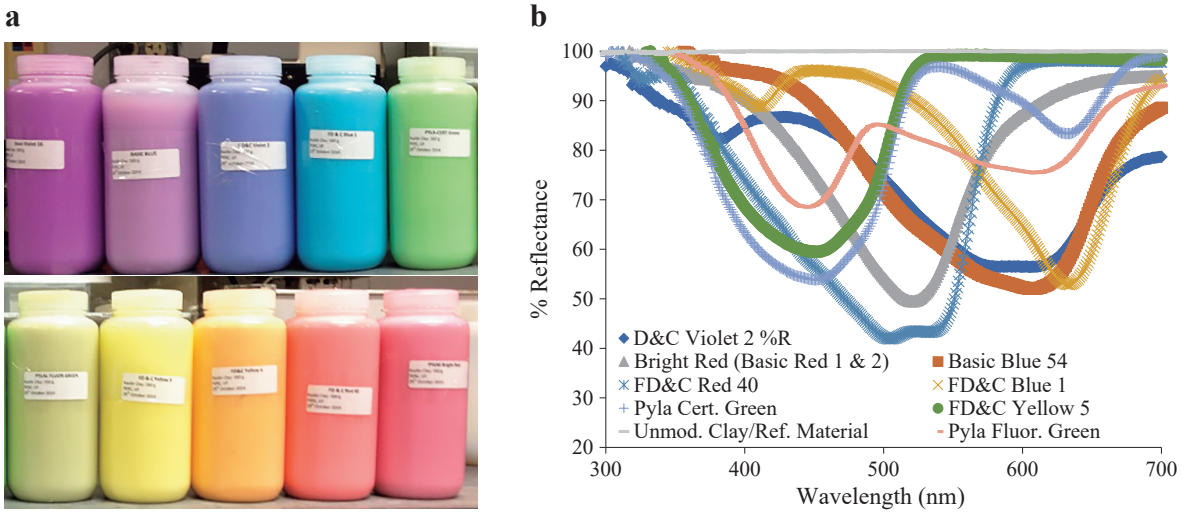

Fig. 6 (a) Colored Kaolin clays developed with surfactants and dyes. **(b)** The reflectance spectrum of the colored clays. Reprinted with permission from Ref. (Moudgil et al., 2017). Copyright: (2017) The Authors, patented in U.S.

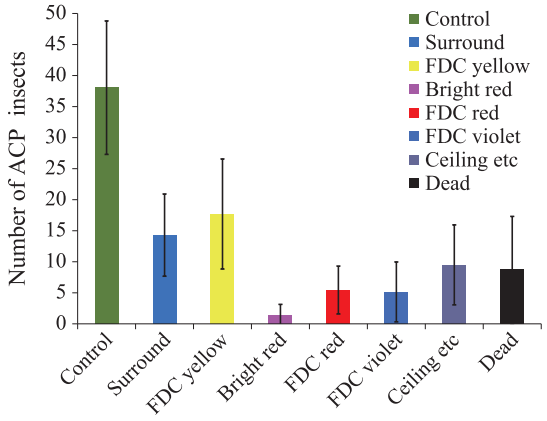

Fig. 7 The choice of ACP to go to the tree coated with different colored clays as compared to Surround® and uncoated leaves. Reprinted with permission from Ref. (Moudgil et al., 2017). Copyright: (2017) The Authors, patented in U.S.

coated leaves was found to depend on the thickness of the coating.

3.7 Effect of the colored coatings on inhibition of Asian Citrus Psyllid (ACP) insect

The selected colored clay formulations were applied to the leaves of citrus plants to deter the Asian Citrus Psyllid *Diaphorina citri*. One hundred psyllids were released in the cage, and they had 24 hours to choose a location before counts were made. **Fig. 7** shows the results from the treatment, and the values are the numbers of psyllids on each tree.

It is observed from **Fig. 7** that ACP has a very low preference for Bright red, followed by FDC red- and violet-colored trees. FDC Yellow clays seem to attract more insects than Surround® coated (white) trees (control). These measurements indicated the potential of colored clay coatings in managing the ACP attack of the fresh flush.

3.8 Rain fastness enhancement

Several formulations were prepared with different adjuvants to determine how well the clay particles adhere to the citrus foliage. Adjuvants were selected based on their ability to act as stickers, binders, or viscosity modifiers. Some of the adjuvants tested resulted in the desorption of the dye from the clays. The colored clay formulations containing Kollicoat, i.e., a pharmaceutical excipient—polyvinyl acetate dispersed in water and stabilized with povidone and sodium dodecyl sulfate, Polymer adjuvant, i.e., sodium polyacrylate, and Xanthan gum yielded coatings with enhanced rain fastness properties.

Several colored clay formulations containing different concentrations of the three adjuvants were sprayed onto the citrus plants, along with white only and colored clays only (no adjuvants) as controls. The coatings were evaluated for color intensity after 1–2, 4–5, and 7 cm of rainfall (see **Fig. 8**). Kollicot and polymer additives were determined to be the best adjuvants for improving both spreading and rain fastness of the colored kaolin clays, withstanding up to 7 cm rain (Moudgil et al., 2017).

3.9 Multimodal contrast agents for cancer detection and treatment

Methods for early detection of cancer using low-cost means remain a critical need. This requires tools that can yield high resolution and sensitivity without compromising the safety of patients. Data from complementary imaging modalities are often evaluated to enable early and accurate detection. Currently employed techniques such as Computed Tomography (CT), Positron Emission Tomography (PET), Magnetic Resonance Imaging (MRI), and Ultrasound possess different detection limits, spatial-temporal resolution, accuracy, and long-term safety upon multiple exposures. However, none of these methods, when

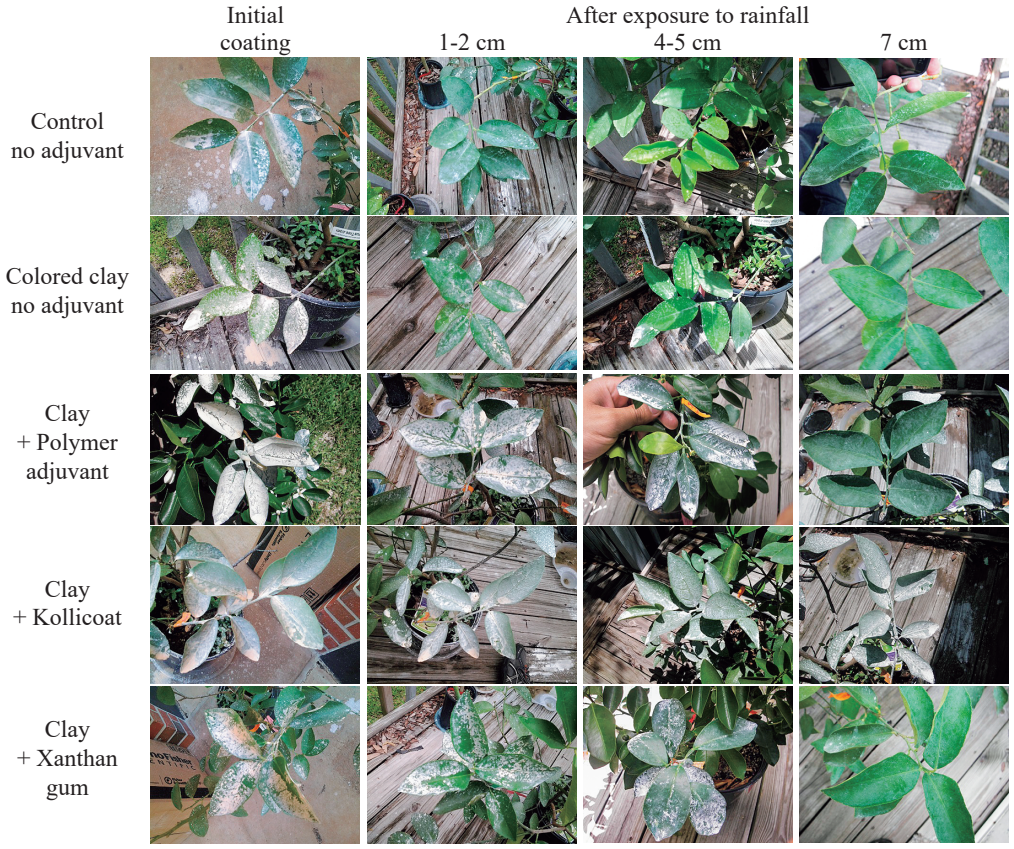

Fig. 8 Images of citrus plants coated with clay, dyed-clay, dyed clay + polymer adjuvant, dyed clay + Kollicoat and dyed clay + Xanthan gum before and after exposure to 1–2 cm, 4–5 cm and 7 cm rainfall. Reprinted with permission from Ref. (Moudgil et al., 2017). Copyright: (2017) The Authors, patented in U.S.

used by themself (alone), yield the required structural and functional information at affordable costs. Availability of safe multimodal—multifunctional contrast agents can promote early detection and treatments. Also, they can enable deep tissue imaging capabilities with some of the currently employed detection tools.

Photo Acoustic tomography (PAT) is a noninvasive imaging technique that employs nonionizing radiation (visible to near-infrared region) to contrast biological tissue and cells. Absorption of "pulsed" incident light by the biological tissue generates an acoustic signal (ultrasound) which is processed to obtain an image of the object. Furthermore, it is possible to image deep tissue because of the lower scattering of the ultrasound waves. However, enhancements in detection are needed for better resolution of the healthy and diseased tissue and cells. Multimodal contrast agents can enhance low-cost imaging using the capabilities of PAT. This may allow high-resolution in vivo imaging of patients with metallic implants who are, otherwise, unable to undergo MRI imaging.

Previously reported attempts to develop contrast agents, although successful but were of limited applicability because of their relatively larger size (120–150 nm). Gold-silica hybrid material termed gold speckled silica (GSS) nanoparticles were synthesized using nonionic water-in-oil (W/O) emulsion technique. An outline of the synthesis protocol is presented below; additional details can be found in the related publications (Hahn et al., 2011; Sharma et al., 2010).

3.10 Synthesis and evaluation of Gd doped GSS nanoparticles as Multimodal contrast agents

The synthesis of the multimodal nanoparticles involved the following steps, (i) preparing the W/O microemulsion by mixing Tx-100 (nonionic surfactant), cyclohexane, and n-hexanol as co-surfactant with the appropriate amount of water. Adding the predetermined amount of TEOS (tetraethyl orthosilicate) in the beginning to the microemulsion and equilibrating the mixture for 30 minutes), (ii) initiating the hydrolysis and polymerization of TEOS by adding NH_4OH. Equilibrating the mixture for 24 hours and adding TSPETE (N-trimethoxysilyl propyl ethylenediamine triacetic acid trisodium salt) and TEOS for modifying the silica nanoparticles, followed by stirring overnight, (iii) adding Gd (III) acetate solution and stirring for another four hours, (iv) adding $HAuCl_4$, and 1.1 M solution of reducing agent (hydrazine hydrate) and stirring for ~12 hours, (v) separating the Gd doped GSS nanoparticles from the micro-emulsion by adding ethanol. Centrifuging the solution to recover nanoparticles of gold, (vi) washing the particles

thoroughly with ethanol and with water to remove surfactant molecules completely. (vii) redispersing the particles in nano-pure water for further characterization. As shown in **Fig. 9**, the gold speckled silica particles (GSS) were 25–60 nm in size, were fluorescent, and exhibited visible NIR absorbance (Sharma et al., 2010). Gd doped GSS particles exhibited unique photothermal properties, which are suitable for PAT imaging and possessing high relaxivity for MRI purposes (Sharma et al., 2012).

Fig. 10 illustrates the following: a) membrane labeled with Alexa Fluor® 488 WGA dye; b) nucleus stained with TO-PRO-3 stain; c) NIR Fluorescence from ICG–SiO_2 nanoparticles; d) an overlay of Fluorescence from the ICG–SiO_2 (pseudo-colored–red) showing the labeling and internalization of the breast cancer cells with the dye-doped nanoparticles. e) Pre-injection epifluorescence image (IVIS, Caliper) of the mouse with 745 nm excitation and 840 nm emission showing minimum background tissue fluorescence; f) NIR fluorescence signal from immediately after the first injection of Gd-doped ICG–SiO_2 nanoparticles showing the increase in signal with minimal interference from the background fluorescence; g) NIR fluorescence immediately following the second injection of Gd-doped ICG nanoparticles. The ROI quantification shows an increase in signal pre- and post-injections.

Gaps in the gold speckled silica surface permit water exchange between the Gd in the silica core and the bulk water, necessary for obtaining an efficient MR contrast. Simultaneously, the metal-dielectric interface generates an efficient PAT contrast enabling the applicability of these particles for diagnostic as well as therapeutic purposes.

Imaging and photothermal ability of the fluorescently doped GSS nanoparticles were evaluated in vitro by injecting GSS nanoparticles intratumorally into nu/nu mice bearing human breast cancers. The tumor region was irradiated with a NIR laser (output 500 mW) for 10 minutes. More than 60 % GSS loaded cells underwent necrotic death as compared to 30 % in control experiments (Sharma et al., 2010). These experiments indicated the suitability of using sub 50 nm NIR absorbing and luminescent GSS nanoparticles for imaging as well as their in-vitro and in-vivo photothermal ablation properties. Further studies were suggested to establish the viability of the GSS type nanoparticles applications for detecting and treating cancerous tissues in practical biological settings.

3.11 Self-stimulating photocatalytic antimicrobial coatings

Contact or touch-based infections are more common than generally recognized. Any contact with common

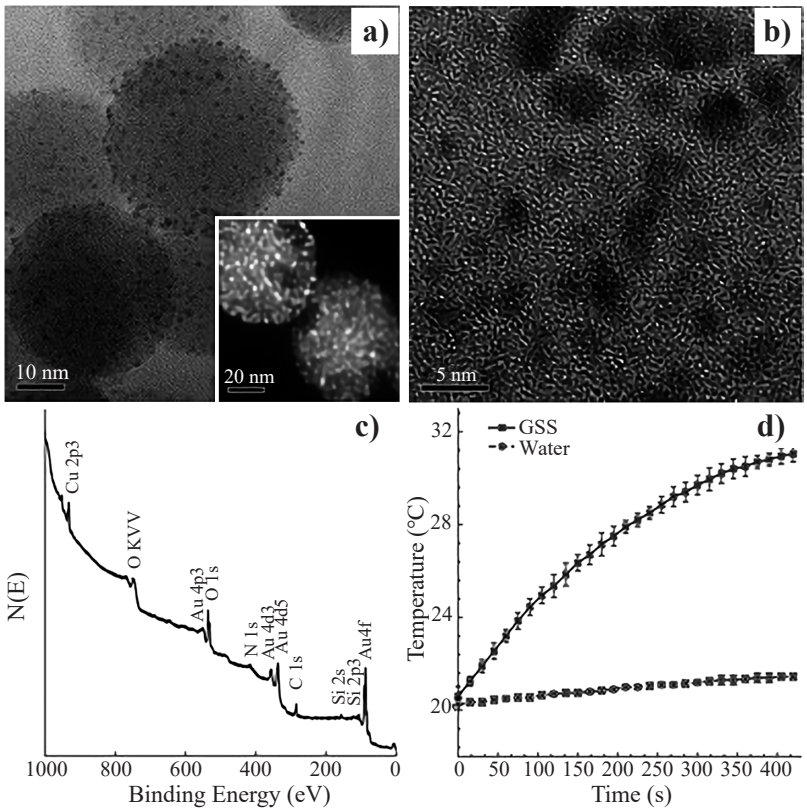

Fig. 9 Characterization of rhodamine doped gold speckled silica (GSS) nanoparticles **(a)** representative TEM image of ca. 40 nm rhodamine doped GSS nanoparticles GSS showing the speckled silica surface; inset Z-contrast digital TEM; **(b)** higher magnification showing irregular shaped, discontinuously placed, 1–5 nm crystalline nano-gold deposits on silica; **(c)** representative XPS spectra; **(d)** ca. 11 °C increase in temperature of pegylated GSS nanoparticles in water suspension. Reprinted with permission from Ref. (Sharma et al., 2010). Copyright: (2010) Royal Society of Chemistry.

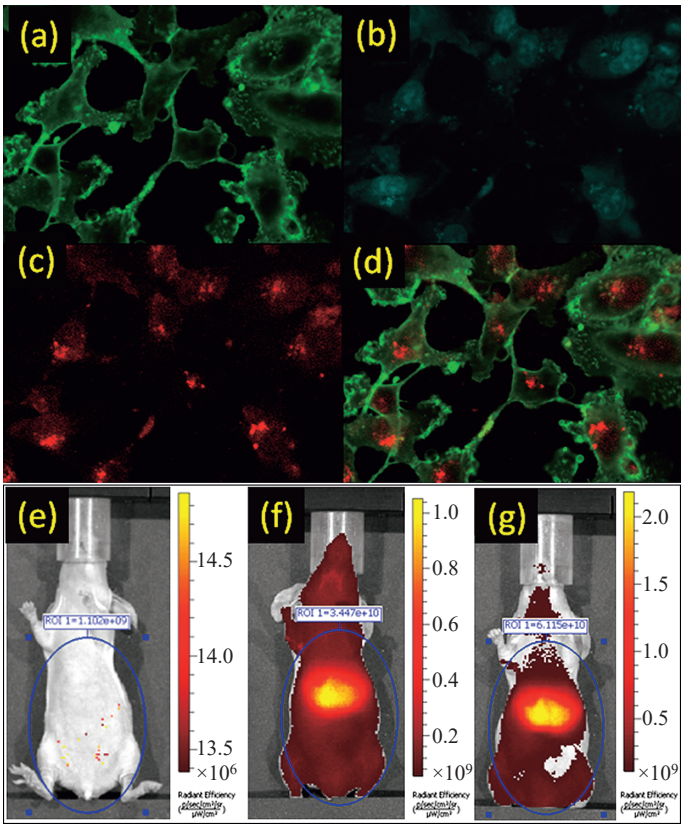

Fig. 10 In vitro and in vivo functional evaluation of ICG–SiO_2 and Gd-doped ICG–SiO_2 nanoparticles. NIR fluorescent image of breast cancer MDA-MB-231 cells. Reprinted with permission from Ref. (Sharma et al., 2012). Copyright: (2012) John Wiley & Sons.

surfaces, including cell phones, keyboards, door handles, clothes, taps, and mops, can transmit infectious microbes. Currently available antimicrobial coatings that slowly release silver or copper ions have a limited lifetime, difficult to employ, and are relatively costly. In contrast, TiO_2 coatings that photo-catalytically mineralize organic contaminants are self-cleaning and produce no toxic by-products, and are relatively inexpensive. However, a major limitation of the TiO_2 by itself has been the need for UV light since, by itself, it exhibits poor photocatalytic properties in visible light.

Among the various techniques investigated for enhancing the photocatalytic property of TiO_2 in visible light include mixing TiO_2 with organic dyes—by far the least complicated method. However, degradation of the dye itself poses a major limitation of this approach. This is attributed to the generation of the reactive oxygen species (ROS) because of the transfer of light-initiated carriers to the TiO_2 surface and their reaction with the surrounding water/oxygen molecules. Interestingly, polyhydroxy fullerenes (PHF) behave the same way as organic dyes and are comparatively more efficient in scavenging electrons. Degradation of the PHF molecules can be tailored by synthesizing the number and placement of hydroxyl groups on the core fullerene structure.

Basic concept: The observation with the dye-sensitized solar cells became the basis of the contaminant-activated photocatalysis concept. It was hypothesized that a dye such as Mordant Orange or Procian Red, when coated on pristine TiO_2, can enhance photocatalysis by absorbing visible light and transferring the generated electrons to the TiO_2 surface. Similarly, when a bacterium such as *Staphylococcus aureus* comes in contact with the TiO_2—dye construct, it should get mineralized. In another scenario, if the bacterium (or any other organic entity) is capable of absorbing the visible light, it should lead to its own degradation ("self-stimulating photocatalytic degradation") by the generated ROS species (Krishna et al., 2018). The organic "contaminant" activated photocatalytic concept, along with measured visible light spectra of various surfaces, with and without different coatings, is presented in **Fig. 11**. Methods, protocols, and tools employed in this research are briefly described below. Additional details are provided by Krishna et al.

3.12 Coating formulations and testing protocols

The preparation of photocatalytic coating formulations involved sonicating 10 mg of anatase in 20 mL water at pH 9.5 for 30 minutes. Rutile and silica coatings, with and without PHF, were prepared in the same fashion. Coating formulations were used for further testing within an hour of their preparation.

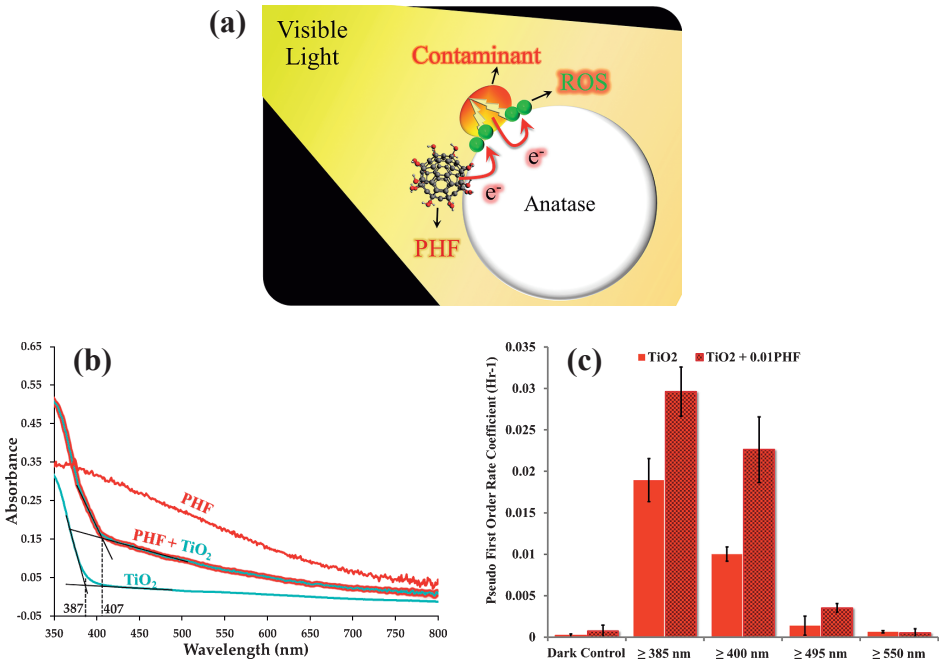

Fig. 11 Contaminant-activated photocatalysis. **(a)** schematic of microbial mineralization with PHF as an auxiliary light harvester. **(b)** Ground-state absorption spectra for anatase (TiO_2), polyhydroxy fullerenes (PHF), and PHF+ TiO_2. **(c)** Pseudo first-order rate coefficients for degradation of Mordant Orange dye on anatase (TiO_2) and anatase + 0.01 (w/w) PHF (TiO_2 + 0.01PHF) coatings. Dark control measures the ability of the photocatalytic coatings to degrade dye in the dark. $N = 10$. Reprinted with permission from Ref. (Krishna et al., 2018). Copyright: (2018) the authors, published by nature, Scientific Reports.

The efficacy of the photocatalytic coatings was tested using ceramic tiles. 0.4 mL of coating formulation was applied to the tile surface and dried for one hour at 40 °C in the dark. Subsequently, the second coat of the same or different coating material was applied. Organic dye or *S. aureus* suspension was applied to the dried surfaces. In *S. aureus*, a suspension (2–3 × 10 CFU/mL) was spread onto each coated tile surface, yielding a surface loading of 6400–9600 CFU/cm. *S. aureus-coated tiles* were dried in the dark in a biosafety cabinet for 3 hours.

3.13 Two-layer coating strategy

First, applying a layer of rutile (or silica) on the surface to be treated, followed by a thin coating of anatase, was devised to protect the base surface from any damage caused by the reactive oxygen species formed due to photocatalysis. Preliminary experiments employing an MRSA surrogate (ATCC 25923) showed promising results.

3.14 Testing in a beta facility

Commercial equipment was employed to apply the coatings, with a commercial primer (BioShield NuTiO) used as the binder between the two coatings. Coated surfaces were tested for antimicrobial efficacy using the bacterial count technique (Krishna et al., 2018). The efficacy of the coatings on various surfaces is illustrated by the results plotted in **Fig. 12**.

It was anticipated that visible light-absorbing organic contaminants, including bacteria and viruses, when in contact with pristine TiO_2 (anatase), can further accelerate the contaminant degradation rate. Considering the wide-ranging applications of TiO_2 in paints, food products, pharmaceuticals, and polymer composites, possible photocatalytic activity aspects should be considered when designing such products (Georgieva et al., 2013; Krishna et al., 2006; Nandakumar et al., 2017; Zhao et al., 2009).

3.15 Inhibition of scale formation by surfactant and polymeric additives

Several industrial processes are adversely impacted by the crystallization of minerals or the formation of "scale" on the surface of the processing equipment. Examples include phosphoric acid manufacturing for fertilizer production, desalination plants, boilers for steam production, and water treatment facilities. Scale deposition severely reduces the process efficiency and requires frequent cleanings that cost money. In phosphoric acid manufacturing, multistage evaporators are frequently used to obtain 52–55 wt % P_2O_5 phosphoric acid. The concentrated phosphoric acid gets supersaturated with respect to calcium sulfate and other scale-forming constituents, which subsequently accumulate on the pipe walls. These deposits reduce the output of the system and require frequent removal to maintain efficiency (Carr et al., 2014). Even a thin layer of deposits can create significant resistance to heat transfer.

Over the last several decades, research attempts have

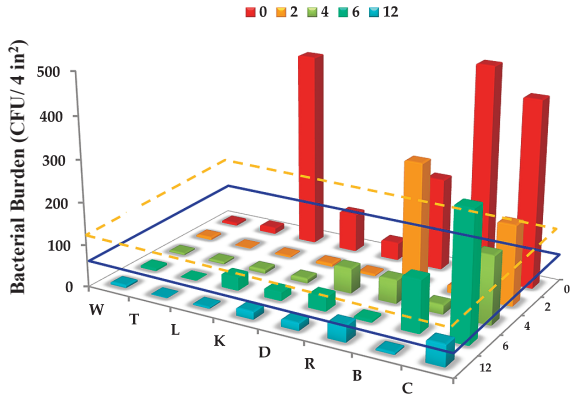

Fig. 12 Beta facility testing. For a given surface, the bars represent counts ($n = 3$) as a function of time from 0 to 12 months. W = Wall; T = Thermostat; L = Locker; K = Knob; D = Soap Dispenser; R = Bathroom Rail; B = Bed Rail; C = Counter. Blue dashed line --the threshold of microbial counts for benign surfaces, and the yellow dashed line - - the average microbial counts on copper surfaces in a clinical trial. Reprinted with permission from Ref. (Krishna et al., 2018). Copyright: (2018) the authors, published by nature, Scientific Reports.

continued to identify the additives that at least might delay the scale formation if not eliminate it outright. In the phosphoric acid production plants, research approaches have focused on the use of water-soluble inhibitors that may block the development of the supercritical nuclei or retard the growth of the calcium sulfate crystals. Several theories have been proposed for antiscaling properties of different additives, but the inhibitors that can perform at a plant scale on a consistent basis have been lacking. Over the last decade, Solvay researchers have developed and demonstrated an antiscalant technology using Phosflow® that substantially reduces the fouling issue in the wet-process phosphoric acid production plants (Carr et al., 2014).

Phosphoric acid is produced by reacting phosphate rock (tricalcium phosphate) with sulfuric acid at high temperatures. This reaction generates calcium sulfate as the byproduct, some of which can deposit on heat exchanger walls when the phosphoric acid is concentrated. Calcium sulfate exists in three forms: calcium sulfate dihydrate, $CaSO_4 \cdot 2H_2O$ (Di-hydrate or DH); calcium sulfate hemihydrate, $CaSO_4 \cdot 0.5H_2O$ (also known as bassanite); and calcium sulfate anhydrous, $CaSO_4$ (anhydrite). Plants generally produce gypsum (calcium sulfate dihydrate) initially, which over time can be baked into anhydrite ($CaSO_4$)—which is dense and difficult to remove (Carr et al., 2014). It has been proposed that in a system supersaturated with DH, first crystals of hemihydrate ($CaSO_4 \cdot 0.5H_2O$ (HH)) precipitate out, which subsequently hydrate into DH. Once the HH crystals are formed, they start to grow into nanorods. At low to medium supersaturation ratios, both bassanite and gypsum crystals seem to form. At high supersaturation ratios, only gypsum precipitates have been observed (no Bassanite). It was further reported that the existence of the precursor phase (bassanite) could be increased by adding carboxylic acid (Polat and Sayan, 2017). Changes in crystal morphology were also observed. Inhibition of scale through the complexation and adsorption of an additive is not unique to $CaSO_4$. A comprehensive review of calcium sulfate precipitation is presented in Driessche et al. (2017).

In order to understand the underlying mechanisms of the Phosflow® (PF) technology, a systematic study was conducted. Turbidity and induction time measurements were used to calculate the inhibition efficiency (E), the surface energy (γ), the nucleation rate (Js), the free energy (ΔG_{cr}), and the critical nucleus size (r). Solubility changes, SEM, FTIR, and XRD, were employed as investigative tools in the in-situ study of how additives affect mineral crystallization on surfaces. It was anticipated that a basic understanding of the scale formation process would allow the development of commercially viable other (greener) additives not only for phosphoric acid plants but also for other systems (Tanquero et al., 2021).

Experimental protocols employed are briefly described below. Reagent grade chemicals, including phosphoric and sulfuric acids, and calcium hydrogen phosphate monobasic $CaH_4(PO_4)^{2-} \cdot 2H_2O$ were purchased from the Fisher Scientific Company and were used as received. Polyethyleneimine of different molecular weights (Mn 0.6 k, 1.8 k, 10 k, and 60 k) was obtained from Sigma Aldrich and Acros Organics Co.

Predetermined volume and ratio of phosphoric and sulphuric acid solutions were added to a 500-mL beaker and heated to 88 °C. The desired amount of calcium phosphate monobasic monohydrate, a specific volume of deionized water or water containing a polymeric additive, along with a corresponding amount of 32.5 g/g (mass%) sulphuric acid was added to the beaker. The reaction temperature was kept constant at 88 °C. The turbidity of the resulting reaction product was measured at different times throughout the reaction using a HACH 2100AN Turbidimeter. Particle Size measurements were conducted using the Accusizer 780 AD. Recovered solids were imaged using an Olympus Optical Microscope.

The effect of PhosFlow (PF) addition is illustrated by **Fig. 13** and data given in **Tables 1** and **2**. PF addition increased the induction time, reduced the surface free energy for nucleation, and delayed the growth of the gypsum (Carr et al., 2014; Tanquero et al., 2021; Zhang L. et al., 2015).

Effects of polymeric additives: Different pathways by which polymeric scale inhibitors can affect nucleation and growth processes include: (a) chelating the active ions in the nucleating solutions (Jamialahmadi and Müller-Steinhagen, 2007); (b) adsorption onto nuclei interfering in nucleation and/or crystal growth (He et al., 1994); (c) dispersion of the scale-forming species (Amjad, 1988); and (d) increasing the local viscosity of the medium thereby affecting the kinetics of the nucleation and growth processes

(Driessche et al., 2017).

Chemical structure, molecular weight, and dosage of additives all are known to govern the efficacy of polymeric type inhibitors (Abdel-Aal et al., 2015; Jain et al., 2019; Akyol et al., 2006). Based on the literature review, three polymeric additives—Poly(acrylic acid) (PAA), Poly(diallyldimethylammonium chloride) (PDADMAC), and Polyethyleneimine (PEI) were selected for the present study. Screening tests revealed that only PEI has the potential of affecting the scale formation in the phosphoric acid system. As shown in **Fig. 14**, PEI effectiveness increased with an increase in polymer molecular weight, and the optimal concentration was determined to be around 40 ppm.

Higher interfacial energies upon PEI addition and morphological changes suggested a plausible mechanism involving adsorption of the polymer molecules on specific crystal faces resulting in inhibition of nuclei growth. Another possibility was stated to be the polymer changing the stability of the precursor molecules, thus prolonging their induction period. The exact role of PEI as a scale inhibitor requires further studies, including monitoring of the structural and morphological changes of the crystals formed, especially during phase changes. In this regard, techniques such as cryo-TEM or small-angle X-ray scattering have been successfully employed to probe molecular-scale mechanisms (Sleutel et al., 2014).

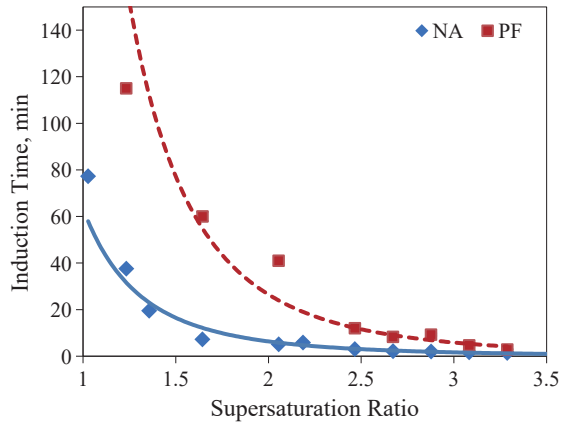

Fig. 13 Effect of PhosFlow (PF) on the induction time as a function of supersaturation ratio. Note: the legend NA and PF represent without additive and with additive PhosFlow, respectively. Reprinted with permission from Ref. (Tanquero et al., 2021). Copyright: (2021) Canadian Journal of Chemical Engineering.

3.16 Surfactant coatings for corrosion inhibition

Corrosion of metal structures, pipelines, boilers, and other industrial equipment is a major challenge in the manufacturing sector. It is estimated by NACE International and other sources that the industrial impact of corrosion

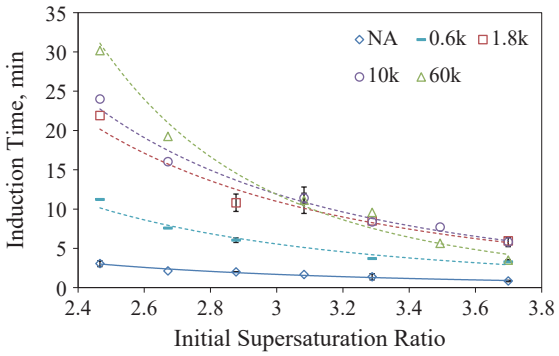

Fig. 14 Effect of PEI molecular weight on the induction time as a function of supersaturation ratio. Reprinted with permission from Ref. (Tanquero et al., 2021). Copyright: (2021) Canadian Journal of Chemical Engineering.

Table 1 Effect of different supersaturation ratio of calcium sulfate on nucleation rate and free energy change for formation of critical nucleus size.

Supersaturation ratio	Nucleation rate J_s 10^{28} nuclei/cm^3·s		Gibbs free energy ΔG 10^{-20} kJ/mol	
	Without PF	With PF	Without PF	With PF 75 ppm
2.466	9.19	22.43	1.19	0.75
2.672	13.35	28.33	1.00	0.63
2.877	17.53	33.60	0.87	0.54
3.083	21.56	38.25	0.76	0.48

Table 2 Effect of different supersaturation ratio of calcium sulfate on critical nucleus size and the number of molecules per a nucleus with and without PF.

Supersaturation ratio	Critical nucleus radius 10^{-8} cm		Number of molecules per a nucleus	
	Without PF	With PF	Without PF	With PF (75 ppm)
2.466	4.68	4.01	5	3
2.672	4.30	3.68	4	3
2.877	4.00	3.42	3	2
3.083	3.76	3.21	3	2

in the US alone is in excess of $500B per year. Corrosion inhibition strategies include designing new materials for corrosion resistance, minimizing contact with corrosive elements, and/or applying protective coatings. The application of organic corrosion inhibitors is quite common in oil and water transport pipelines. Surfactant blends constitute most of the corrosion inhibitors.

Most of the effective inhibitors comprise heteroatoms such as O, N, S, and π bonds, which enable them to attach to the metal surface (Bockris et al., 2000). The specific chemical nature of a given corrosion inhibitor (CI) depends on the environment (nature of ions, pH, temperature, etc.). Organic corrosion inhibitors, especially surface-active agents (surfactants), have been reported to be some of the most effective inhibitors due to their ability to form self-assembled films at interfaces, as shown in **Fig. 15** (Fuchs-Godec, 2009; Zhu et al., 2016; 2017). These barrier layers inhibit the transport of corrosion, causing ionic species to and from the surface.

Despite their advantages and wide usage, the scientific understanding of corrosion inhibition using surfactants at the molecular level is not comprehensive. One of the major aims of the current research was to characterize the surfactant films formed on the steel surface to gain a better understanding of the corrosion inhibition mechanism. A brief description of the materials, methods and experimental protocols is outlined below. Additional details can be found elsewhere (Rajopadhye, 2018).

The standard practice for laboratory immersion corrosion testing of metals (ASTM G31) was followed to prepare the test samples. AISI1010 carbon steel rod (Obtained from McMaster-Carr, composition: C 0.13 %, Mn 0.4 %, P 0.04 %, S 0.05 % and balance Fe) was used to fabricate the working electrode. A circular rod of the cross-section area of 0.08 cm^2 (accurate within ±1 %) was coated in epoxy resin such that only the circular cross-section of the rod at the end was exposed to the electrolyte while immersed in the test solution. The exposed end of the steel rod was polished using 600, 800, 1000, and 1200 grit silicon carbide abrasive pads to remove the surface oxide layer, followed by fine polishing using 1 μ colloidal silica slurry and diamond paste. The RMS surface roughness of the polished specimen was determined to be ~25 nm using AFM surface topography. The steel specimen thus prepared was degreased by sonicating in ethanol followed by thorough rinsing using DI water and dried by the jet of nitrogen gas. The steel surface thus prepared was exposed to the test solution no later than 30 minutes after the polishing was done in order to keep surface oxidation to a minimum level.

The surfactants investigated in this study were purchased from Sigma-Aldrich (research-grade) and were used as received. All the surfactant solutions were prepared by adding the calculated amounts of surfactants to triple distilled DI water (Resistivity of 18.1 MΩ.cm) to prepare the stock solutions. These stock solutions were used to prepare the desired concentration by successive dilutions.

All the electrochemical investigations were performed in a standard 3-electrode electrochemical cell, Multiport™ (supplied by Gamry Instruments Inc.), connected to the Reference3000™ potentiostat (Model number 20215, supplied by Gamry Instruments Inc.) equipped with an inbuilt lock-in amplifier. The saturated calomel electrode (SCE) housed inside the Luggin capillary was used as a reference electrode, whereas a high-density graphite rod was used as an auxiliary electrode. 800 mL of test solution was transferred to the Gamry Multiport™ electrochemical cell after the solution pH was adjusted. The cell was closed by placing the glass lid with a Viton O-ring to seal the vessel. All the tests were performed at 25 ± 1 °C. The temperature of the test solutions was maintained by circulating water through the jacket around the electrochemical cell. All experiments were repeated multiple times to ensure the reproducibility of the data.

3.17 Effect of nature of the surfactant head group on corrosion inhibition

In an attempt to isolate the effect of the head group chemical nature, octadecyl trimethyl ammonium bromide (OTAB) was selected as a counterpart to oleic imidazoline (OI), an active ingredient in commercial corrosion inhibitor

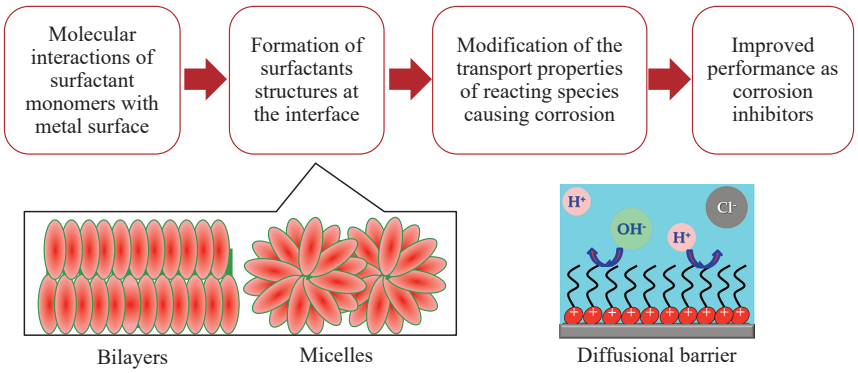

Fig. 15 Self-assembled surfactant structure as a diffusional barrier to the transport of corrosion causing species. Reprinted with permission from Ref. (Rajopadhye, 2018). Copyright: (2018) University of Florida.

blends. They both have 18 carbon atoms in their hydrocarbon chain, albeit different chain structures—OTAB straight chain: OI with a double bond in the hydrocarbon chain. The inhibition efficiency of the two surfactants was determined to be 78 % vs. 83 % for OI and OTAB, respectively, indicating that the contributions from the two polar head groups are relatively well matched.

3.18 Effect of hydrophobic interactions on corrosion inhibition

The corrosion inhibition contribution of the hydrophobic effects due to the chain-chain interactions was investigated by comparing the inhibition performances of different inhibitors with the same head group chemistry but varying chain lengths. Several homologous members (from 10 to 18 CH_2 groups) of quaternary ammonium bromide (TAB) were tested at the same bulk concentration for their corrosion inhibition efficiency. It was determined that the corrosion rate decreased with an increase in the hydrocarbon chain length. Both corrosion rate and the polarization resistance are plotted as a function of hydrocarbon chain length in **Fig. 16**.

The observed results can be explained based on the degree of surface activity of the surfactant molecules. Higher surface activity due to higher chain length results in higher and probably denser surface coverage, thereby providing more corrosion protection. Therefore, in spite of the same number of molecules being present in the bulk solution for each surfactant, better corrosion protection was provided by OTAB as compared to DTAB since a higher number of OTAB molecules are expected to be adsorbed at the interface due to their higher surface activity, thereby blocking a greater number of active sites for corrosion.

3.19 Effect of surfactant concentration

Comparison of the corrosion inhibition efficiency as a function of DTAB and OI concentration in **Fig. 17** revealed that optimal corrosion inhibition occurs at a lower concentration than their respective critical micelle concentration (CMC) values. OI was determined to be more effective than DTAB, possibly due to the stronger electrochemical interaction of the imidazoline ring with the steel surface resulting in more effective corrosion protection.

The initial part with the higher slope in both the plots represents the region where the corrosion rate is increasingly reduced as more and more active sites are blocked by the adsorbed inhibitor molecules. This region is fairly straight-lined, indicating that the corrosion inhibition is directly proportional to the surface coverage by the surfactant molecules. The second part, also almost straight-lined, albeit with a relatively lower slope, indicates almost complete coverage of the surface with monolayer and/or surfactant aggregate structures. The corrosion protection in this region was attributed to the blocking of the active corrosion sites as well as the resistance to the transport of corrosive species through the surfactant aggregates.

The inflection point in each plot represents a structural change in the adsorbed layer from monolayer to multilayer (bilayers or micelles!). Concentration at the inflection

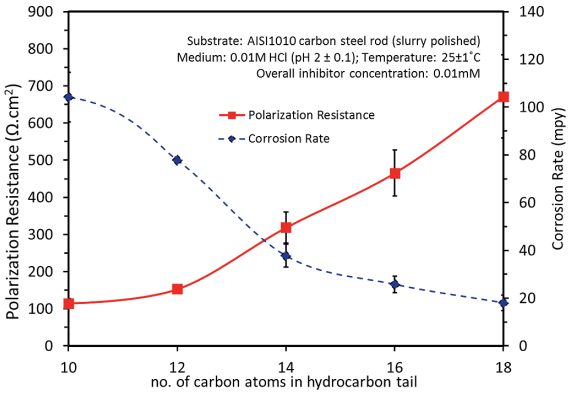

Fig. 16 Corrosion rate (CR) and the polarization resistance (*R*p) for AISI1010 carbon steel exposed to 0.01 M HCl solution in the presence of the homologous series of TAB inhibitors at 0.01 mM concentration at 298 K. Reprinted with permission from Ref. (Rajopadhye, 2018). Copyright: (2018) University of Florida.

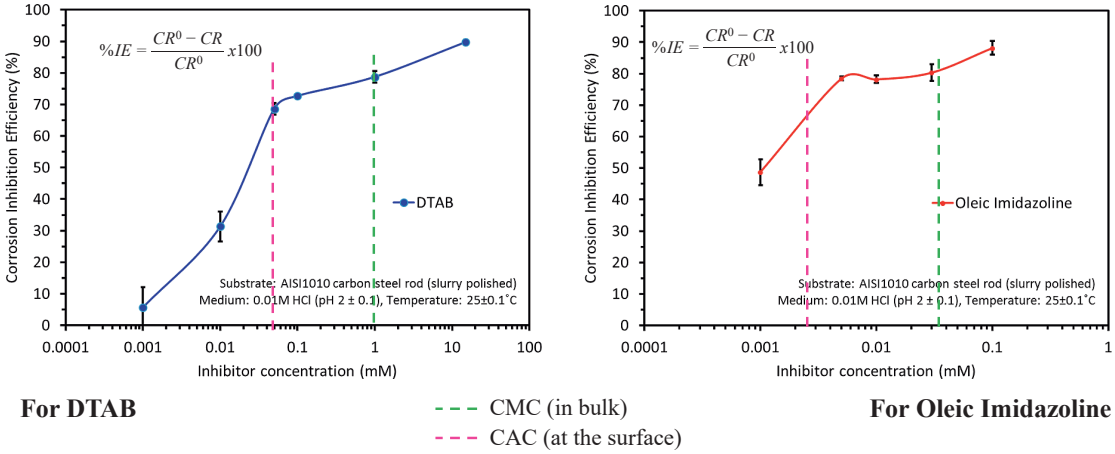

Fig. 17 Comparison of corrosion inhibition efficiency of DTAB and OI as a function of concentration. Reprinted with permission from Ref. (Rajopadhye, 2018). Copyright: (2018) University of Florida.

point is termed as the critical aggregate concentration (CAC), the concentration at which the aggregate structures start forming at the interface. The CAC value for DTAB (0.05 mM) is about an order of magnitude higher than for OI (CAC = 0.005 mM). This could be due to the higher surface activity of OI molecules as compared to DTAB as a result of differences in their hydrocarbon chain lengths. Interestingly, the CAC values (CAC_{DTAB} = 0.07 mM and CAC_{OI} = 0.008 mM) are lower than the bulk CMCs of the two surfactants (CMC_{DTAB} = 15 mM and CMC_{OI} = 0.03 mM), indicating the possibility of the metal surface catalyzing the self-structuring process resulting in the aggregation taking place on the surface (CAC) at a lower concentration than in bulk (CMC) (Singh et al., 2001).

3.20 Surfactant adsorption mechanism

The mode of adsorption for the OI-type additives has been reported to be chemical in nature. In the present study, adsorption of DTAB and OI was determined to obey the Langmuir adsorption isotherm. The free energy calculations of 9.3 kJ/mol for DTAB and 9.4 kJ/mol for OI are more indicative of the physical adsorption mechanism. The literature reports are inconclusive in this regard (Keera et al., 2012; Zhu et al., 2015; 2017). Further investigations are required to reach a conclusive determination about the adsorption mechanism of the most effective corrosion inhibitors.

Overall, the two key contributions to corrosion inhibition – physical (the hydrophobic interactions between the chains) and electrochemical (the head group interactions with the surface) were isolated in this study by varying one component while keeping the other constant. It was demonstrated that the physical contributions play an equally important role in determining the corrosion inhibition properties of the surfactant-based inhibitors. The chain-chain interactions of surfactant molecules that drive them to the interface determine the number of surfactant molecules available for adsorption and thus dictate the overall surface coverage and the corrosion inhibition efficiency.

3.21 Precision gold nanoparticles synthesis

Precision particles of very narrow size distribution, especially metal (e.g., gold) nanoparticles, are needed for advanced sensor applications and as reference materials for toxicology assessments. Additional commercial applications of such particles are limited due to their high cost. Narrowly sized gold nanoparticles (AuNPs) can cost up to $10,000 per gram AuNPs. One of the major reasons for their high cost is their labor-intensive batch production which is susceptible to batch-to-batch variation. The aim of this project was to develop a continuous production technique that is scalable for cost-effectively and high-throughput production of precise metal nanoparticles. AuNPs can be synthesized using the Turkevich method. The average particle size, size distribution, and morphology were characterized by UV-visible spectroscopy, Dynamic Light Scattering (DLS), and Transmission Electron Microscopy (TEM). Chemical composition was analyzed with XPS, FT-IR, and ICP-MS Spectrometry. The precision of nanoparticles, i.e., size distribution, was quantified using the polydispersity index, PDI (ISO13321, 1996).

Over the last decades, nanoparticle synthesis using flow chemistry has attracted more attention because of its automation capability and potential for low-cost production of high-precision nanomaterials (Nightingale et al., 2014; Stitt, 2002). Typical flow chemistry involves the mixing of reactants in a chip-based microfluidic cell under specific conditions (Wagner et al., 2008). However, relatively low throughput and reactor fouling are some of the major limitations of microfluidic reactors for nanoparticle synthesis. Moreover, attempts to scale up such reactors often lead to the loss of precision control of the particle properties such as the size and size distribution.

In this study, initial efforts to produce narrowly sized gold nanoparticles using a single-phase flow reactor were unsuccessful primarily due to reactor fouling. The attempts to overcome reactor fouling by changing the reactor material, flow rate, and particle synthesis chemistry were not successful. However, these attempts revealed that most likely fouling was caused by heterogeneous nucleation and the growth of gold on the reactor surface. Fouling in continuous nanoparticle synthesis can be overcome in carefully designed two-phase or biphasic flow systems that comprise two immiscible fluids. In the biphasic reactor, the continuous phase is selected such that it preferentially wets the reactor surface, and the dispersed phase consists of reactant solution. In the present study, silicone oil was selected as the continuous phase since it was expected to wet the reactor surface, Perfluoro alkoxy, or PFA tubing. Gold chloride ($HAuCl_4$) and trisodium citrate ($Na_3C_6H_5O_7$) constituted the two aqueous phase reactants. A schematic of the flow reactor is illustrated in **Fig. 18**.

As shown in **Fig. 19**, silicone oil was introduced from both sides of the cross-junction (IDEX, ETFE P-723) as the continuous phase and droplets of aqueous reactants were generated when the already mixed solution of the two reactants was merged into the silicone oil. Each aqueous droplet dispersed in the silicone oil acted as an individual mini reactor. Additional experimental details can be found in the publication (Dong et al., 2022). It is important that the system conditions of concentrations, flow rate, and temperature, and pressure are controlled such that the aqueous reagents are completely mixed during their flow in the channel before the mixed reactants are discharged/dispersed into the non-aqueous phase. It should be noted that to avoid nucleation before complete mixing of the reactants, the channel temperature is maintained at room

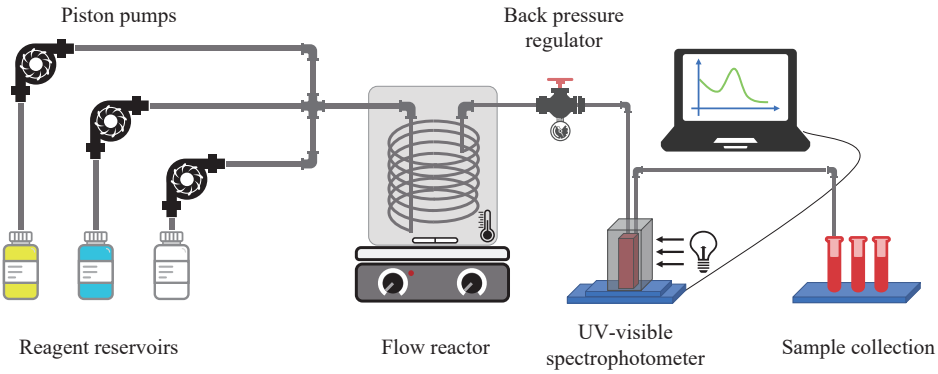

Fig. 18 The layout of the flow reactor system used for gold nanoparticle synthesis. Reprinted with permission from Ref. (Dong et al., 2022). Copyright: (2022) The Authors, published by KONA Powder and Particle Journal.

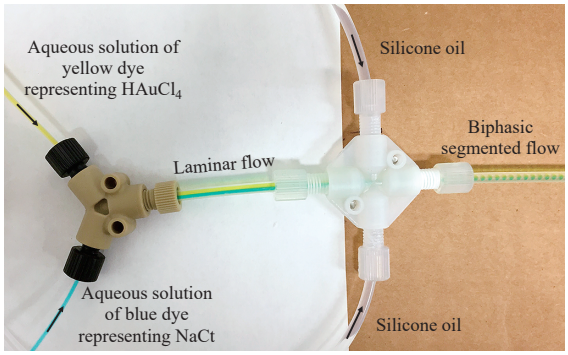

Fig. 19 Experimental setup showing the generation of liquid-liquid biphasic segmented flow. The yellow and blue dye represent $HAuCl_4$ and NaCt solutions, respectively. Reprinted with permission from Ref. (Dong et al., 2022). Copyright: (2022) The Authors, published by KONA Powder and Particle Journal.

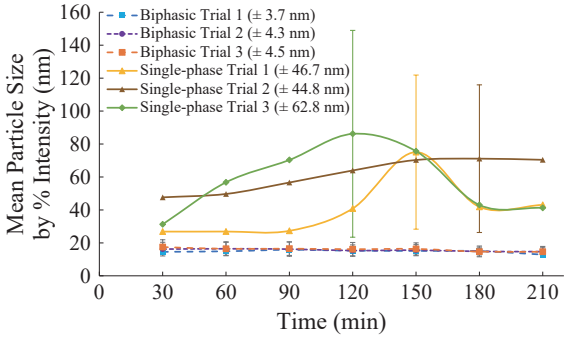

Fig. 20 DLS measurement of the mean particle size of the AuNPs synthesized in biphasic flow reactor. Reprinted with permission from Ref. (Dong et al., 2022). Copyright: (2022) The Authors, published by KONA Powder and Particle Journal.

temperature to slow the precipitation reaction kinetics; and to accelerate the kinetic process, the droplets of the mixed reactants are heated to 100 °C as soon as they are dispersed in the non-aqueous phase.

No fouling was observed in the biphasic flow reactor. Moreover, as indicated in **Figs. 20** & **21**, the gold nanoparticles produced were consistent over several hours of biphasic reactor operation. This was attributed to the elimination of fouling and the much more efficient mixing of the reactants due to the recirculating flow fields encountered inside of each aqueous segment/droplet dispersed in the continuous fluid. The precision of the nanoparticles produced was determined by calculating the polydispersity index (PDI) values. Polydispersibility index values of the gold nanoparticles (PDI = 0.068) were determined to be very close to the PDI of the reference material generated in batch synthesis (PDI = 0.065). Overall, it was determined that fouling in the continuous flow reactors can be overcome by avoiding the nucleation reaction in the vicinity of the reactor surface; otherwise, it could impact the particle properties and the reaction yield.

4. Concluding remarks

Although there have been considerable advances in particle synthesis, functionalization, characterization, and performance assessment methodologies, a number of challenges remain that need to be overcome before large-scale applications of engineered particulate systems become a reality. Some of the challenges and opportunities, especially related to the fields of research discussed in this paper, are outlined below.

In the area of particle assisted microbe adhesion and removal from household surfaces, skin, bio-implants, hospital and general use fabrics, etc. in the form of sprays & coatings, controlled release devices, and wipes, there is a critical need for a better understanding of the mechanisms of bacterial interactions with different types of surfaces and engineered particulates including polymers, inorganic, metal, skin, etc. (D'Accolti et al., 2018; Varshney et al., 2021). Qualitative or semi-quantitative information about the mode of microbial adhesion exists, but there is a lack of quantitative data on the various forces involved in microbial adhesion and removal. Reliable data is needed to develop robust modeling and simulation schemes. Specifically, in the handwashing applications field, reducing the time it takes to wash off the microbial contaminants below

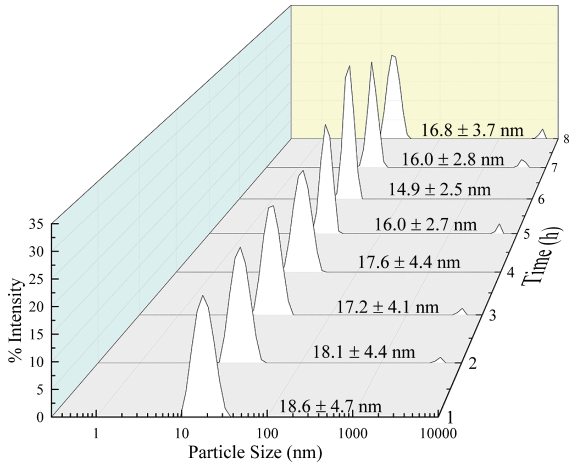

Fig. 21 DLS measurements of particle size and size distribution of gold nanoparticle samples synthesized using liquid-liquid biphasic flow reactor. The particle size and size distribution remained constant in the 8-hours uninterrupted experiment. Reprinted with permission from Ref. (Dong et al., 2022). Copyright: (2022) The Authors, published by KONA Powder and Particle Journal.

a safe threshold is an important goal. Furthermore, developing suitable hand hygiene, body cleansing formulations, and detergency for water-stressed regions of the world is fast becoming an acute necessity.

Large-scale applications of particulate coatings for crop protection require low-cost functionalized materials such as clays for foliar applications not only for protection from insects but also for on-demand delivery of actives and micronutrients to the plants. Moreover, functionalized particles must not cause any harmful effects to crop quality and yield. Multifunctional particle formulations and smart aggregates for on-demand delivery purposes can help reduce the dependence on chemicals that might otherwise result in the generation of antibiotic-resistant microbes. Selective killing of only harmful insects and bacteria, leaving the healthy microbes and insects intact, remains a prized long-term goal.

On the particulate systems mediated disinfectant front using photocatalytic coatings, considerable progress has been made in identifying suitable doping additives to enhance photocatalysis under visible light. However, the low rate of disinfection requiring relatively longer disinfection times remains a major competitive disadvantage for large-scale applications. Additionally, nanotoxicity continues to be a challenge for titania-based disinfection coatings (Jafari et al., 2020; Liao et al., 2020; Rtimi et al., 2019). Bismuth oxide coatings have been reported to outperform other photocatalytic materials, including titania. However, long exposure times are required for microbial inactivation (Ratova et al., 2018). For the disinfection of surfaces, increasing the efficacy of applied coatings to reduce the frequency of disinfectant applications is a critical need.

Practical application of surfactants for corrosion inhibition has been a theme of several studies not only to enhance the effectiveness of current formulations but also to develop greener surfactant coatings (Sliem et al., 2019; Zhuang et al., 2021). Facilities for testing the efficacy of formulations under field conditions of high temperature, pressure, salinity, pH, flow conditions and particulate contamination, etc., are scarce. Suggestions for setting up a flow loop incorporating above mentioned parameters should yield the data needed for developing robust predictive models (Zhu et al., 2017).

Biomedical applications of nanoparticles continue to be a strong driver for advanced applications of engineered particulate systems for the detection and treatment of cancer. Several comprehensive review articles have summarized the latest developments in this regard. Despite the positive outlook, major challenges need to be overcome before large-scale clinical implementation of such materials becomes a reality. These include toxicity, long term biodistribution, biodegradability, in addition to protocols for large scale production of multimodal particles at low cost (Aghebati-Maleki et al., 2020; Gallo et al., 2013; Han et al., 2019; Hsu et al., 2020; Luo et al., 2021; Silva et al., 2019; Thanapandiyaraj et al., 2018).

Despite several studies across the globe, the toxicity of nanoparticles continues to be a major obstacle for their large-scale usage in biomedical, consumer goods, healthcare, and pharmaceutical products. Lack of availability of well-characterized reference materials for conducting comprehensive toxicological assessments has been a problem for industrial and academic researchers alike. In the USA, the National Institute of Environmental Health Sciences (NIEHS) has funded several groups to generate the required data. Most recently, NIEHS funded a consortium led by the Center for Nanotechnology and Nanotoxicology, T.H. Chan School of Public Health, Harvard University in collaboration with MIT, University of Maine, and the University of Florida to create a repository of well-characterized engineered nanomaterials for toxicological studies. Availability of precise nanoparticles (narrowly sized and/or with specifically designed functionalities) at low cost, however, remains a barrier because of batch production of such particles that invariably involves numerous iterations to generate modest quantities of narrowly sized nanoparticles thereby driving up their prices. In this regard, biphasic continuous flow reactors have shown promise pending their successful scale up for larger-scale production (Dong et al., 2022).

In recent years, AI has become a popular tool for complex materials and systems design, simulation, and optimization. For example, Shams et al. employed AI methods to estimate and optimize the silver nanoparticle concentration on the treated silk fabrics for antimicrobial properties (Shams Nateri et al., 2019). Vinoth and Datta used the artificial neural network and genetic algorithm to

design a novel nanoparticle reinforced polymer composite for replacements in hip joints (Vinoth and Datta, 2020). Mahmoud et al. implemented the artificial neural network to simulate and predict the removal efficiency of several organic contaminates from aqueous systems using iron nanoparticle sorbents (Mahmoud et al., 2018).

AI techniques have also been utilized in various biomedical applications, including image inspection via machine learning, histopathology examination, making unbiased medical decisions, molecular and medicine performance modeling (Chaddad et al., 2021; Jin et al., 2020). AI has the ability to precisely detect nanoparticle biomarkers or contrast agents in biological systems from medical imaging modalities (Zhang et al., 2021). It also has the potential to predict and model the property and response of a hypothetical contrast agent in specific systems. The main limitation of AI applications remains the lack of professional data curation and quality assurance (Bi et al., 2019). Other challenges include validating the predictive AI models, understanding the fundamental mechanisms of the AI models, and reaching a consensus in the research community about the AI outcomes (Bi et al., 2019).

Greater interactions among the industry and academic researchers not only would advance the field of particle and powder technology-mediated processes and products but also help create a well-trained cadre of sorely needed young researchers and practitioners in the field. Additionally, meaningful collaborations among physical scientists and engineers, life scientists, and clinicians are necessary to develop nanoparticle-based sensors, multimodal contrast agents, and other health monitoring and treatment devices. Overall, in the last few decades, there have been tremendous advances in the field, and more exciting new discoveries are expected in the coming years, especially with the advent of AI-mediated particulate systems-related innovations.

Acknowledgments

The authors convey special thanks to Dr. P. Sharma, Dr. V. Krishna, Dr. V. Nandakumar, and Dr. J. Tanquero for their valuable assistance with some of the figures incorporated in this paper. The authors acknowledge the financial support of the National Science Foundation Center for Particulate and Surfactant Systems (CPaSS) and the industry members (NSF Award #1362060, NSF Award #1602032). Any opinions, findings, and conclusions or recommendations expressed in this material are those of the authors and do not necessarily reflect the views of the National Science Foundation or the CPaSS industry members.

References

Abdel-Aal E.A., Abdel-Ghafar H.M., El Anadouli B.E., New findings about nucleation and crystal growth of reverse osmosis desalination scales with and without inhibitor, Crystal Growth and Design, 15 (2015) 5133–5137. DOI: 10.1021/acs.cgd.5b01091

Aghebati-Maleki A., Dolati S., Ahmadi M., Baghbanzhadeh A., Asadi M., Fotouhi A., Yousefi M., Aghebati-Maleki L., Nanoparticles and cancer therapy: perspectives for application of nanoparticles in the treatment of cancers, Journal of Cellular Physiology, 235 (2020) 1962–1972. DOI: 10.1002/jcp.29126

Akyol E., Bozkurt A., Öner M., The effects of polyelectrolytes on the inhibition and aggregation of calcium oxalate crystallization, Polymers for Advanced Technologies, 17 (2006) 58–65. DOI: 10.1002/pat.693

Amjad Z., Calcium sulfate dihydrate (gypsum) scale formation on heat exchanger surfaces: the influence of scale inhibitors, Journal of Colloid and Interface Science, 123 (1988) 523–536. DOI: 10.1016/0021-9797(88)90274-3

Badr M.S.H., Yuan S., Dong J., El-Shall H., Bermudez Y.A., Ortega D.C., Lopez-Rendon J.E., Moudgil B.M., The properties of Kaolin from different locations and their impact on casting rate, KONA Powder and Particle Journal, 38 (2021) 251–259. DOI: 10.14356/kona.2021002

Basim G.B., Vakarelski I.U., Moudgil B.M., Role of interaction forces in controlling the stability and polishing performance of CMP slurries, Journal of Colloid and Interface Science, 263 (2003) 506–515. DOI: 10.1016/S0021-9797(03)00201-7

Behl S., Moudgil B.M., Prakash T.S., Control of active sites in selective flocculation. I. Mathematical model, Journal of Colloid and Interface Science, 161 (1993) 414–421. DOI: 10.1006/jcis.1993.1483

Behl S., Willis M.J., Young R.H., Colored titaniferous coating pigment obtained as a flocculated by-product in a kaolin purification process, United States Patent, (1996) US5584394A.

Bellon-Fontaine M.N., Rault J., van Oss C.J., Microbial adhesion to solvents: a novel method to determine the electron-donor/electron-acceptor or Lewis acid-base properties of microbial cells, Colloids and Surfaces B: Biointerfaces, 7 (1996) 47–53. DOI: 10.1016/0927-7765(96)01272-6

Bi W.L., Hosny A., Schabath M.B., Giger M.L., Birkbak N.J., Mehrtash A., Allison T., Arnaout O., Abbosh C., Dunn I.F., Mak R.H., Tamimi R.M., Tempany C.M., Swanton C., Hoffmann U., et al., Artificial intelligence in cancer imaging: clinical challenges and applications, CA: A Cancer Journal for Clinicians, 69 (2019) 127–157. DOI: 10.3322/caac.21552

Bockris J.O'M., Reddy A.K.N., Gamboa-Aldeco M.E., Modern Electrochemistry 2A-Fundamentals of Electrodics, Springer New York LLC, 2000, ISBN: 9780306461675. DOI: 10.1007/b113922

Carr J., Zhang L., Davis M., Ravishankar S.A., Flieg G., Scale controlling chemical additives for phosphoric acid production plants, Procedia Engineering, 83 (2014) 233–242. DOI: 10.1016/j.proeng.2014.09.043

Chaddad A., Katib Y., Hassan L., Future artificial intelligence tools and perspectives in medicine, Current Opinion in Urology, 31 (2021) 371–377. DOI: 10.1097/MOU.0000000000000884

D'Accolti M., Soffritti I., Piffanelli M., Bisi M., Mazzacane S., Caselli E., Efficient removal of hospital pathogens from hard surfaces by a combined use of bacteriophages and probiotics: potential as sanitizing agents, Infection and Drug Resistance, 11 (2018) 1015–1026. DOI: 10.2147/IDR.S170071

Dong J., Lau J., Svoronos S.A., Moudgil B.M., Continuous synthesis of precision gold nanoparticles using a flow reactor, KONA Powder and Particle Journal, 39 (2022) 2022011. DOI: 10.14356/kona.2022011

Driessche A.E.S., Stawski T.M., Benning L.G., Kellermeier M., Calcium sulfate precipitation throughout its phase

diagram, In: Van Driessche A., Kellermeier M., Benning L., Gebauer D. (eds), New Perspectives on Mineral Nucleation and Growth. Springer, Cham., 2017, pp. 227–256. DOI: 10.1007/978-3-319-45669-0_12

El-Shall H., Moudgil B.M., El-Midany A., Separation of ink particles from waste paper by fine-bubbles, KONA Powder and Particle Journal, 23 (2005) 122–128. DOI: 10.14356/kona.2005015

Fuchs-Godec R., Effects of surfactants and their mixtures on inhibition of the corrosion process of ferritic stainless steel, Electrochimica Acta, 54 (2009) 2171–2179. DOI: 10.1016/j.electacta.2008.10.014

Gallo J., Long N.J., Aboagye E.O., Magnetic nanoparticles as contrast agents in the diagnosis and treatment of cancer, Chemical Society Reviews, 42 (2013) 7816–7833. DOI: 10.1039/c3cs60149h

Gao J., Krishna V., Bai W., Koopman B.L., Moudgil B.M., Indeglia P.A., Folta K.M., Georgieva A.T., Functionalized fullerenes as a biomass stimulant and a life extension agent, United States Patent, (2016) US9399756B2.

Gao J., Wang Y., Folta K.M., Krishna V., Bai W., Indeglia P., Georgieva A., Nakamura H., Koopman B., Moudgil B., Polyhydroxy fullerenes (fullerols or fullerenols): beneficial effects on growth and lifespan in diverse biological models, PLoS ONE, 6 (2011) 19976–19985. DOI: 10.1371/journal.pone.0019976

Georgieva A.T., Pappu V., Krishna V., Georgiev P.G., Ghiviriga I., Indeglia P., Xu X., Fan Z.H., Koopman B., Pardalos P.M., Moudgil B., Polyhydroxy fullerenes, Journal of Nanoparticle Research, 15 (2013) 1690. DOI: 10.1007/s11051-013-1690-6

Glenn D.M., Puterka G.J., Chapter 1- Particle films: a new technology for agriculture, in: Janick J. (Ed.), Horticultural Reviews, 2004, pp. 1–44. DOI: 10.1002/9780470650882.ch1

Glenn D.M., The mechanisms of plant stress mitigation by kaolin-based particle films and applications in horticultural and agricultural crops, HortScience Horts, 47 (2012) 710–711. DOI: 10.21273/hortsci.47.6.710

Grafton-Cardwell E.E., Stelinski L.L., Stansly P.A., Biology and management of Asian citrus psyllid, vector of the huanglongbing pathogens, Annual Review of Entomology, 58 (2013) 413–432. DOI: 10.1146/annurev-ento-120811-153542

Hahn M.A., Singh A.K., Sharma P., Brown S.C., Moudgil B.M., Nanoparticles as contrast agents for in-vivo bioimaging: current status and future perspectives, Analytical and Bioanalytical Chemistry, 399 (2011) 3–27. DOI: 10.1007/s00216-010-4207-5

Hamadi F., Latrache H., Comparison of contact angle measurement and microbial adhesion to solvents for assaying electron donor–electron acceptor (acid–base) properties of bacterial surface, Colloids and Surfaces B: Biointerfaces, 65 (2008) 134–139. DOI: 10.1016/J.COLSURFB.2008.03.010

Han X., Xu K., Taratula O., Farsad K., Applications of nanoparticles in biomedical imaging, Nanoscale, 11 (2019) 799–819. DOI: 10.1039/c8nr07769j

He S., Oddo J.E., Tomson M.B., The inhibition of gypsum and barite nucleation in NaCl brines at temperatures from 25 to 90 °C, Applied Geochemistry, 9 (1994) 561–567. DOI: 10.1016/0883-2927(94)90018-3

Hsu J.C., Nieves L.M., Betzer O., Sadan T., Noël P.B., Popovtzer R., Cormode D.P., Nanoparticle contrast agents for X-ray imaging applications, Wiley Interdisciplinary Reviews: Nanomedicine and Nanobiotechnology, 12 (2020) e1642. DOI: 10.1002/WNAN.1642

ISO13321, Methods for determination of particle size distribution part 8: photon correlation spectroscopy, International Organisation for Standardisation (ISO), (1996).

Jafari S., Mahyad B., Hashemzadeh H., Janfaza S., Gholikhani T., Tayebi L., Biomedical applications of TiO_2 nanostructures: recent advances, International Journal of Nanomedicine, 15 (2020) 3447–3470. DOI: 10.2147/IJN.S249441

Jain T., Sanchez E., Owens-Bennett E., Trussell R., Walker S., Liu H., Impacts of antiscalants on the formation of calcium solids: implication on scaling potential of desalination concentrate, Environmental Science: Water Research & Technology, 5 (2019) 1285–1294. DOI: 10.1039/C9EW00351G

Jamialahmadi M., Müller-Steinhagen H., Heat exchanger fouling and cleaning in the dihydrate process for the production of phosphoric acid, Chemical Engineering Research and Design, 85 (2007) 245–255. DOI: 10.1205/cherd06050

Jin P., Ji X., Kang W., Li Y., Liu H., Ma F., Ma S., Hu H., Li W., Tian Y., Artificial intelligence in gastric cancer: a systematic review, Journal of Cancer Research and Clinical Oncology, 146 (2020) 2339–2350. DOI: 10.1007/s00432-020-03304-9

Keera S.T., Farid N.A., Mohamed K.Z., Imidazoline derivatives as corrosion inhibitors of carbon steel in crude oils and associated water, Energy Sources, Part A: Recovery, Utilization and Environmental Effects, 34 (2012) 1371–1383. DOI: 10.1080/15567036.2010.481657

Krishna V., Bai W., Han Z., Yano A., Thakur A., Georgieva A., Tolley K., Navarro J., Koopman B., Moudgil B., Contaminant-activated visible light photocatalysis, Scientific Reports, 8 (2018) 1894. DOI: 10.1038/s41598-018-19972-0

Krishna V., Moudgil B., Koopman B., Systems and methods based on radiation induced heating or ignition of functionalized fullerenes, United States Patent, (2016a) US9475028B2.

Krishna V., Moudgil B., Koopman B., Functionalized fullerenes as antifungal agents, United States Patent, (2016b) US9314027B2.

Krishna V., Noguchi N., Koopman B., Moudgil B., Enhancement of titanium dioxide photocatalysis by water-soluble fullerenes, Journal of Colloid and Interface Science, 304 (2006) 166–171. DOI: 10.1016/j.jcis.2006.08.041

Krishna V., Stevens N., Koopman B., Moudgil B., Optical heating and rapid transformation of functionalized fullerenes, Nature Nanotechnology, 5 (2010) 330–334. DOI: 10.1038/nnano.2010.35

Krishna V., Zawoy K., Moudgil B.M., Koopman B.L., Stevens N.I., Powers K.W., Devices for thermally induced transformations controlled by irradiation of functionalized fullerenes, United States Patent, (2015) US9011309B2.

Liao C., Li Y., Tjong S.C., Visible-light active titanium dioxide nanomaterials with bactericidal properties, Nanomaterials, 10 (2020) 124 (56pp). DOI: 10.3390/nano10010124

Luo D., Wang X., Burda C., Basilion J.P., Recent development of gold nanoparticles as contrast agents for cancer diagnosis, Cancers, 13 (2021) 1825 (16pp). DOI: 10.3390/cancers13081825

Mahmoud A.S., Mostafa M.K., Abdel-Gawad S.A., Artificial intelligence for the removal of benzene, toluene, ethyl benzene and xylene (BTEX) from aqueous solutions using iron nanoparticles, Water Science and Technology: Water Supply, 18 (2018) 1650–1663. DOI: 10.2166/ws.2017.225

Mehta N, Flocculation Behavior of Apatite with Polyacrylic Acid, MS Thesis, University of Florida, Gainesville, FL, 1993.

Moudgil B.M., Musella S.C., Etxeberria E., Rogers M.E., Brodersen C.R., Sharma P., Colored clays for agricultural and other industrial applications, United States Patent, (2017) US9763440B2.

Nandakumar V., Physicochemical Aspects of Bacterial Adhesion on Surfaces and Strategies to Remove Adhered

Bacteria from Surfaces, Doctoral Dissertation, University of Florida, Gainesville, FL, 2018. https://ufdc.ufl.edu/UFE0052040/00001

Nandakumar V., Han Z., Fritz Z., Krishna V., Koopman B., Moudgil B., Visible light photocatalytic bacterial inactivation on titanium dioxide coatings, KONA Powder and Particle Journal, 34 (2017) 234–240. DOI: 10.14356/kona.2017011

Nandakumar V., Huang C., Pulgar A., Balasubramanian V., Wu G., Chandar P., Moudgil B.M., Particle assisted removal of microbes from surfaces, Journal of Colloid and Interface Science, 533 (2019) 190–197. DOI: 10.1016/j.jcis.2018.08.043

Narayanan A., Sharma P., Moudgil B.M., Applications of engineered particulate systems in agriculture and food industry, KONA Powder and Particle Journal, 30 (2012) 221–235. DOI: 10.14356/kona.2013021

Nightingale A.M., Phillips T.W., Bannock J.H., De Mello J.C., Controlled multistep synthesis in a three-phase droplet reactor, Nature Communications, 5 (2014) 3777. DOI: 10.1038/ncomms4777

Owens D.K., Wendt R.C., Estimation of the surface free energy of polymers, Journal of Applied Polymer Science, 13 (1969) 1741–1747. DOI: 10.1002/app.1969.070130815

Polat S., Sayan P., Determination of the effects of carboxylic acids on calcium sulfate dihydrate crystallization, Chemical Engineering and Technology, 40 (2017) 1354–1361. DOI: 10.1002/ceat.201600525

Prakash T.S., Moudgil B.M., Removal of chloride and potassium ions from the recovery boiler salt cake, in: TAPPI Proceedings—International Environmental Conference, 1995, pp. 161–174, ISBN:0898529360.

Puterka G.J., Glenn D.M., Pluta R.C., Action of particle films on the biology and behavior of pear psylla (Homoptera: Psyllidae), Journal of Economic Entomology, 98 (2005) 2079–2088. DOI: 10.1093/jee/98.6.2079

Rabinovich Y.I., Adler J.J., Esayanur M.S., Ata A., Singh R.K., Moudgil B.M., Capillary forces between surfaces with nanoscale roughness, Advances in Colloid and Interface Science, 96 (2002) 213–230. DOI: 10.1016/S0001-8686(01)00082-3

Rabinovich Y.I., Vakarelski I.U., Brown S.C., Singh P.K., Moudgil B.M., Mechanical and thermodynamic properties of surfactant aggregates at the solid-liquid interface, Journal of Colloid and Interface Science, 270 (2004) 29–36. DOI: 10.1016/j.jcis.2003.09.005

Rajopadhye A., Understanding the Fundamental Role of Surfactant Structures in the Inhibition of Carbon Steel Corrosion in Acidic Medium, Doctoral Dissertation, University of Florida, Gainesville, FL, 2018. https://ufl-flvc.primo.exlibrisgroup.com/permalink/01FALSC_UFL/175ga98/alma990366927060306597

Ratova M., Redfern J., Verran J., Kelly P.J., Highly efficient photocatalytic bismuth oxide coatings and their antimicrobial properties under visible light irradiation, Applied Catalysis B: Environmental, 239 (2018) 223–232. DOI: 10.1016/j.apcatb.2018.08.020

Rtimi S., Dionysiou D.D., Pillai S.C., Kiwi J., Advances in catalytic/photocatalytic bacterial inactivation by nano Ag and Cu coated surfaces and medical devices, Applied Catalysis B: Environmental, 240 (2019) 291–318. DOI: 10.1016/j.apcatb.2018.07.025

Shams Nateri A., Hasanlou E., Hajipour A., Using adaptive neuro-fuzzy and genetic algorithm for simultaneously estimating the dye and AgNP concentrations of treated silk fabrics with nanosilver, Pigment and Resin Technology, 48 (2019) 20–28. DOI: 10.1108/PRT-11-2017-0096

Sharma P., Bengtsson N.E., Walter G.A., Sohn H.B., Zhou G., Iwakuma N., Zeng H., Grobmyer S.R., Scott E.W., Moudgil B.M., Gadolinium-doped silica nanoparticles encapsulating indocyanine green for near infrared and magnetic resonance imaging, Small, 8 (2012) 2856–2868. DOI: 10.1002/smll.201200258

Sharma P., Brown S.C., Singh A., Iwakuma N., Pyrgiotakis G., Krishna V., Knapik J.A., Barr K., Moudgil B.M., Grobmyer S.R., Near-infrared absorbing and luminescent gold speckled silica nanoparticles for photothermal therapy, Journal of Materials Chemistry, 20 (2010) 5182–5185. DOI: 10.1039/c0jm00354a

Sharma P., Moudgil B.M., Walter G.A., Grobmyer S.R., Santra S., Jiang H., Brown S.C., Scott E.W., Zhang Q., Bengtsson N., Multimodal nanoparticles for non-invasive bio-imaging, United States Patent, (2013a) US8361437B2.

Sharma P., Narayanan A., El-Shall H.E., Moudgil B.M., Engineered particulate systems for controlled release of pesticides and repellants, WIPO (PCT), (2013b) WO2013123176A1.

Sharma P., Brodersen C., Rogers M., Etxeberria E., Optical and physical deterrent for preventing ACP vector attack on citrus, Citrus Research and Development Foundation (CRDF), CATP13 Proposal #860, Gainesville, United States, 2015.

Silva C.O., Pinho J.O., Lopes J.M., Almeida A.J., Gaspar M.M., Reis C., Current trends in cancer nanotheranostics: metallic, polymeric, and lipid-based systems, Pharmaceutics, 11 (2019) 22 (40pp). DOI: 10.3390/pharmaceutics11010022

Singh A., Krishna V., Angerhofer A., Do B., MacDonald G., Moudgil B., Copper coated silica nanoparticles for odor removal, Langmuir, 26 (2010) 15837–15844. DOI: 10.1021/la100793u

Singh P.K., Adler J.J., Rabinovich Y.I., Moudgil B.M., Investigation of self-assembled surfactant structures at the solid-liquid interface using FT-IR/ATR, Langmuir, 17 (2001) 468–473. DOI: 10.1021/la000981t

Sleutel M., Lutsko J., Van Driessche A.E.S., Durán-Olivencia M.A., Maes D., Observing classical nucleation theory at work by monitoring phase transitions with molecular precision, Nature Communications, 5 (2014) 5598. DOI: 10.1038/ncomms6598

Sliem M.H., Afifi M., Bahgat Radwan A., Fayyad E.M., Shibl M.F., Heakal F.E.-T., Abdullah A.M., AEO7 surfactant as an eco-friendly corrosion inhibitor for carbon steel in HCl solution, Scientific Reports, 9 (2019) 2319 (16pp). DOI: 10.1038/s41598-018-37254-7

Stitt E.H., Alternative multiphase reactors for fine chemicals: a world beyond stirred tanks?, Chemical Engineering Journal, 90 (2002) 47–60. DOI: 10.1016/S1385-8947(02)00067-0

Tanquero J.G., Abdel-Aal E.-S.A., Farinato R.S., El-Shall H., Moudgil B.M., Inhibition of calcium sulphate hemihydrate crystallization under simulated conditions of phosphoric acid evaporation, The Canadian Journal of Chemical Engineering, (2021). DOI: 10.1002/cjce.24210

Thanapandiyaraj R., Rajendran T., Mohammedgani P.B., Performance analysis of various nanocontrast agents and CAD systems for cancer diagnosis, Current Medical Imaging Formerly Current Medical Imaging Reviews, 15 (2018) 831–852. DOI: 10.2174/1573405614666180924124736

Varshney S., Sain A., Gupta D., Sharma S., Factors affecting bacterial adhesion on selected textile fibres, Indian Journal of Microbiology, 61 (2021) 31–37. DOI: 10.1007/s12088-020-00903-5

Vinoth A., Datta S., Design of the ultrahigh molecular weight polyethylene composites with multiple nanoparticles: an artificial intelligence approach, Journal of Composite Materials,

54 (2020) 179–192. DOI: 10.1177/0021998319859924
Wagner J., Tshikhudo T.R., Köhler J.M., Microfluidic generation of metal nanoparticles by borohydride reduction, Chemical Engineering Journal, 135 (2008) S104–S109. DOI: 10.1016/j.cej.2007.07.046
Wenninger E.J., Stelinski L.L., Hall D.G., Roles of olfactory cues, visual cues, and mating status in orientation of Diaphorina citri Kuwayama (Hemiptera: Psyllidae) to four different host plants, Environmental Entomology, 38 (2009) 225–234. DOI: 10.1603/022.038.0128
Zhang H., Meng D., Cai S., Guo H., Chen P., Zheng Z., Zhu J., Zhao W., Wang H., Zhao S., Yu J., He Y., The application of artificial intelligence in lung cancer: a narrative review, Translational Cancer Research, 10 (2021) 2478–2487. DOI: 10.21037/tcr-20-3398
Zhang L., Carr J., Chen T.H.-L., Primary amine-containing polymers useful as scale inhibitors, WIPO (PCT), (2015) WO2015123294A1.
Zhang X., Zhang Q., Yan T., Jiang Z., Zhang Xinxin, Zuo Y.Y., Quantitatively predicting bacterial adhesion using surface free energy determined with a spectrophotometric method, Environmental Science and Technology, 49 (2015) 6164–6171. DOI: 10.1021/es5050425
Zhao J., Krishna V., Hua B., Moudgil B., Koopman B., Effect of UVA irradiance on photocatalytic and UVA inactivation of Bacillus cereus spores, Journal of Photochemistry and Photobiology B: Biology, 94 (2009) 96–100. DOI: 10.1016/j.jphotobiol.2008.10.006
Zhu Y., Free M.L., Woollam R., Durnie W., A review of surfactants as corrosion inhibitors and associated modeling, Progress in Materials Science, 90 (2017) 159–223. DOI: 10.1016/j.pmatsci.2017.07.006
Zhu Y., Free M.L., Yi G., Experimental investigation and modeling of the performance of pure and mixed surfactant inhibitors: aggregation, adsorption, and corrosion inhibition on steel pipe in aqueous phase, Journal of The Electrochemical Society, 162 (2015) C582–C591. DOI: 10.1149/2.09415010jes
Zhu Y., Free M.L., Yi G., The effects of surfactant concentration, adsorption, aggregation, and solution conditions on steel corrosion inhibition and associated modeling in aqueous media, Corrosion Science, 102 (2016) 233–250. DOI: 10.1016/j.corsci.2015.10.012
Zhuang W., Wang X., Zhu W., Zhang Y., Sun D., Zhang R., Wu C., Imidazoline Gemini surfactants as corrosion inhibitors for carbon steel X70 in NaCl solution, ACS Omega, 6 (2021) 5653–5660. DOI: 10.1021/acsomega.0c06103

Authors' Short Biographies

Jiaqi Dong

Jiaqi Dong received his B.S. in Materials Science and Engineering from the Illinois Institute of Technology in 2013. He then attended the University of Florida as a graduate student and received his M.S. in Materials Science and Engineering in 2016. Currently, he is a Ph.D. candidate under the supervision of Dr. Brij Moudgil and Dr. Bahar Basim at the Center for Particulate and Surfactant Systems (CPaSS). His current research focus is metallic nanoparticle synthesis and functionalization using flow chemistry.

Brij M. Moudgil

Dr. Brij M. Moudgil is a Distinguished Professor of Materials Science and Engineering at the University of Florida. He received his B.E from the Indian Institute of Science, Bangalore, India, and his M.S. and Eng.Sc.D degrees from Columbia University, New York. His current research interests are in surfactant and polymer adsorption, dispersion and aggregation of fine particles, adhesion, and removal of microbes from surfaces, synthesis of functionalized nanoparticles, anti-scaling and surfactant mediated corrosion inhibitors, photocatalytic degradation of hazardous microbes, and nanotoxicity. He has published more than 400 technical papers and has been awarded over 25 patents. He is a member of the U.S National Academy of Engineering.